NeuroImage 64 (2013) 308–327

Contents lists available at SciVerse ScienceDirect

NeuroImage

journal homepage: www.elsevier.com/locate/ynimg

Task-related component analysis for functional neuroimaging and application to near-infrared spectroscopy data

Hirokazu Tanaka [*,1,2], Takusige Katura [**,1], Hiroki Sato

Central Research Laboratory, Hitachi, Ltd., 2520 Akanuma, Hatoyama, Saitama 350-0395, Japan

ARTICLE INFO

Article history:
Accepted 16 August 2012
Available online 24 August 2012

Keywords:
Correlation maximization
Covariance maximization
Functional neuroimaging
Optical topography
Biomedical data analysis
Rayleigh–Ritz problem

ABSTRACT

Reproducibility of experimental results lies at the heart of scientific disciplines. Here we propose a signal processing method that extracts task-related components by maximizing the reproducibility during task periods from neuroimaging data. Unlike hypothesis-driven methods such as general linear models, no specific time courses are presumed, and unlike data-driven approaches such as independent component analysis, no arbitrary interpretation of components is needed. Task-related components are constructed by a linear, weighted sum of multiple time courses, and its weights are optimized so as to maximize inter-block correlations (CorrMax) or covariances (CovMax). Our analysis method is referred to as task-related component analysis (TRCA). The covariance maximization is formulated as a Rayleigh–Ritz eigenvalue problem, and corresponding eigenvectors give candidates of task-related components. In addition, a systematic statistical test based on eigenvalues is proposed, so task-related and -unrelated components are classified objectively and automatically. The proposed test of statistical significance is found to be independent of the degree of autocorrelation in data if the task duration is sufficiently longer than the temporal scale of autocorrelation, so TRCA can be applied to data with autocorrelation without any modification. We demonstrate that simple extensions of TRCA can provide most distinctive signals for two tasks and can integrate multiple modalities of information to remove task-unrelated artifacts. TRCA was successfully applied to synthetic data as well as near-infrared spectroscopy (NIRS) data of finger tapping. There were two statistically significant task-related components; one was a hemodynamic response, and another was a piece-wise linear time course. In summary, we conclude that TRCA has a wide range of applications in multichannel biophysical and behavioral measurements.

Introduction

Analysis of neuroimaging data can be in general classified into two categories: a hypothesis-driven approach such as general linear models (GLMs), and a data-driven approach such as principle component analysis (PCA) and independent component analysis (ICA). Hypothesis- and data-driven approaches correspond to supervised and unsupervised approaches, respectively, in machine learning. In the hypothesis-driven approach, a single time course obtained in neuroimaging data is assumed to consist of certain specific task-related components (e.g., hemodynamic responses) and task-unrelated components (e.g., systemic signals and head movement artifacts). In GLMs, these presumed components are summarized in a so-called design matrix, and their contributions are statistically assessed by the statistical parametric mapping (SPM) method (Friston et al., 1994b). For analysis of functional magnetic resonance imaging (fMRI) data, GLM and SPM have been highly successful in localizing voxels that show significant activations related to a task. The GLM analysis, however, requires certain hypotheses about task-related and task-unrelated components, which may not be a priori obvious in some cases such as the shape of hemodynamic response function (Plichta et al., 2007). Furthermore, GLM is not able to assess components that are not modeled into a design matrix.

Another approach to neuroimaging data analysis is the data-driven approach in which only general statistical assumptions are made to decompose neuroimaging data. One notable example is ICA, in which only statistical independence between source signals is assumed (Amari et al., 1996; Bell and Sejnowski, 1995; Hyvarinen and Oja, 1997). ICA extracts independent components as a linear weighted sum of multiple time series and maximizes some information-theoretic criteria such as mutual information or higher-order cumulants. ICA has been successfully applied to fMRI, electroencephalography (EEG) and near-infrared spectroscopy (NIRS) data analyses (Katura et al., 2008; Kohno et al., 2007; Makeig et al., 1996; McKeown and Sejnowski, 1998). In contrast to GLM, ICA makes no assumptions other than statistical independence

* Corresponding author. Fax: +81 761 51 1149.
** Corresponding author. Fax: +81 49 296 5999.
E-mail addresses: hirokazu@jaist.ac.jp (H. Tanaka), takusige.katura.ny@hitachi.com (T. Katura).
[1] Equally contributed.
[2] Present address: Japan Advanced Institute of Science and Technology, 1-1 Asahidai, Nomi, Ishikawa 923-1211, Japan.

1053-8119/$ – see front matter
http://dx.doi.org/10.1016/j.neuroimage.2012.08.044

between source signals, so it can sometimes discover unexpected components in neuroimaging data. Moreover, its applicability is not limited to neuroimaging data but also covers physiological and behavioral data (Nakamura et al., 2004). Independent components discovered by ICA, however, need an additional process for determining which of independent components are task-related or artifactual (Nakada et al., 2000). Also, due to its generality, the original formulation of ICA does not make any use of available information regarding experimental procedures (there are a few extensions of ICA that incorporate temporal or spatial constraints, though; Calhoun et al., 2005; Lin et al., 2010).

We here propose a new analysis approach to extract task-related components from a linear weighted sum of multiple time series. This analysis will be referred to as *task-related component analysis* (TRCA). Coefficients, or weights, of time series are determined so as to maximize the covariance or correlation between task blocks, thereby maximizing the inter-block consistency. This is based on a belief that a signal that appears consistently and robustly in every task block should be regarded as task related. In other words, we define task relatedness by consistent and robust appearance of a same signal. This covariance-maximization problem is formulated as a Rayleigh–Ritz eigenvalue problem, and statistical significance of each solution can be assessed by a corresponding eigenvalue. Unlike GLM, TRCA assumes no a priori knowledge of time series other than task periods, and unlike ICA, TRCA can provide a concrete measure of task-relatedness to each extracted component. In GLM analyses, autocorrelation in time series poses a serious issue of inflated statistics, but we show that TRCA is not sensitive to autocorrelation if the time scale of temporal smoothing is smaller than the duration of task block. Furthermore, we show that TRCA can be generalized into a classification problem of binary tasks and can sequentially incorporate known effects obtained from an additional source such as respiration and body motion in order to remove task-unrelated artifacts. We illustrate our proposed method by applying to synthetic data and NIRS data. Although our method has been developed mainly for NIRS data analysis, we argue that it has a wide applicability to multi-channel physiological and behavioral measurements.

Methods

The 'Signal reconstruction from weighted linear summation' section illustrates a linear generative model of observed time courses and explains the concept that covariance maximization can recover task-related components. The 'Task-related component analysis: a basic formulation' section formulates TRCA by using two conventional measures; a correlation coefficient and covariance, and the 'Statistical test of task consistency' section proposes a statistical test for choosing significantly task-related components. The 'Effect of temporal smoothing and autocorrelation' section argues how autocorrelation due to temporal smoothing affects results of the statistical test. The 'Task-distinctive components' and 'Data augmentation' sections explain simple extensions of our method for multiple tasks and for data augmentation, respectively. These extensions are not easily realized with PCA or ICA. The 'Mapping of a task-related component' section argues how to obtain a spatial map of task-related component. Finally, 'Application to synthetic data' and 'NIRS finger tapping experiment' sections summarize details of synthetic and NIRS data. Further tests of the methods are described in the supplementary data.

Signal reconstruction from weighted linear summation

We here illustrate the concept of task-related component analysis by a simple example. Two signal sources are assumed when there are three blocks of a task; one ($s(t)$: task related) that has the same profile during every task block (i.e., $s^{(1)}(t)$, $s^{(2)}(t)$ and $s^{(3)}(t)$ are the same, sustained wave forms) (Fig. 1A, top), and another ($n(t)$: task unrelated) that is flat except the second block (i.e., $n^{(2)}(t)$ is phasic whereas $n^{(1)}(t)$ and $n^{(3)}(t)$ are flat) (Fig. 1A, bottom). These signal time courses are constructed so that covariance -between blocks of the task-related component is a positive constant ($\mathrm{Cov}(s^{(1)}(t),s^{(2)}(t))=\mathrm{Cov}(s^{(1)}(t),s^{(3)}(t))=\mathrm{Cov}(s^{(2)}(t),s^{(3)}(t))=$ positive const) whereas covariance between blocks of the task-unrelated component and between task-related and task-unrelated are zero ($\mathrm{Cov}(s^{(i)}(t),n^{(j)}(t))=\mathrm{Cov}(n^{(i)}(t),n^{(j)}(t))=0$ $(1\le i<j\le 3)$). A linear generative model of observed time courses ($x_1(t)$ and $x_2(t)$) are assumed as

$$\begin{cases} x_1(t) = a_{11}s(t) + a_{12}n(t) \\ x_2(t) = a_{21}s(t) + a_{22}n(t) \end{cases}, \tag{1}$$

as illustrated in Fig. 1B. The problem is to recover the latent task related component $s(t)$ from a linear sum of observed time courses defined as

$$y(t) = w_1x_1(t) + w_2x_2(t) = (w_1a_{11} + w_2a_{21})s(t) + (w_1a_{12} + w_2a_{22})n(t). \tag{2}$$

We propose to maximize the covariance of the first-block ($y(1)(t)$) and the second-block ($y(2)(t)$) time courses (here, for simplicity, covariance between first and second blocks is considered, and a multiple-block case will be discussed in the following subsection):

$$\begin{aligned}\mathrm{Cov}\left(y^{(1)},y^{(2)}\right) &= (w_1a_{11}+w_2a_{21})^2\mathrm{Cov}\left(s^{(1)},s(2)\right) \\ &\quad +(w_1a_{12}+w_2a_{22})^2\mathrm{Cov}\left(n^{(1)},n(2)\right) \\ &\quad +(w_1a_{11}+w_2a_{21})(w_1a_{12}+w_2a_{22})\left[\mathrm{Cov}\left(s^{(1)},n(2)\right)\right. \\ &\quad \left.+\,\mathrm{Cov}\left(n^{(1)},s(2)\right)\right] \\ &= (w_1a_{11}+w_2a_{21})^2\mathrm{Cov}\left(s^{(1)},s(2)\right).\end{aligned} \tag{3}$$

Here we used $\mathrm{Cov}(n^{(1)},n^{(2)})=\mathrm{Cov}(s^{(1)},n^{(2)})=\mathrm{Cov}(n^{(1)},s^{(2)})=0$. This is a quadratic function of w_1 and w_2, which is unbounded. To obtain a finite solution, the variance of $y(t)$ is constrained to be one,

$$\mathrm{var}(y) = (w_1a_{11} + w_2a_{21})^2 + (w_1a_{12} + w_2a_{22})^2 = 1, \tag{4}$$

where the signals are assumed to be normalized ($\mathrm{Var}(s(t))=\mathrm{Var}(n(t))=1$) and uncorrelated ($\mathrm{Cov}(s(t),n(t))=0$). This constrained optimization problem has a solution of $w_1a_{11}+w_2a_{21}=1$ and $w_1a_{12}+w_2a_{22}=0$, leading to the final solution $y(t)=s(t)$ unless $a_{11}a_{22}-a_{12}a_{21}=0$. This simple example suggests that inter-block covariance maximization can be a guiding principle for reconstructing task-related components from observed time courses. The following sections will discuss general multiple time-course cases.

Task-related component analysis: a basic formulation

Suppose that N-channel temporal signals denoted by $x_i(t)$ $(i=1,\ldots,N)$ are given, containing K blocks of a same repeated task whose periods are fixed as $t\in[t_k,t_k+T]$ $(k=1,\cdots,K)$. Here T is duration of each task block. We propose that a task-related component is computed as a linear, weighted sum of those input signals as:

$$y(t) = \sum_{i=1}^{N} w_i x_i(t) = \mathbf{w}^{\mathrm{T}}\mathbf{x}(t). \tag{5}$$

As in the previous section, we implicitly assume that observed signals are generated by a linear weighted sum of task-related and task-unrelated components so that task-related components can be recovered by appropriately weighing observed signals. The goal of this analysis is to optimize the coefficients in such a way that a temporal profile of a task-related component exhibits a maximal temporal similarity among task blocks,

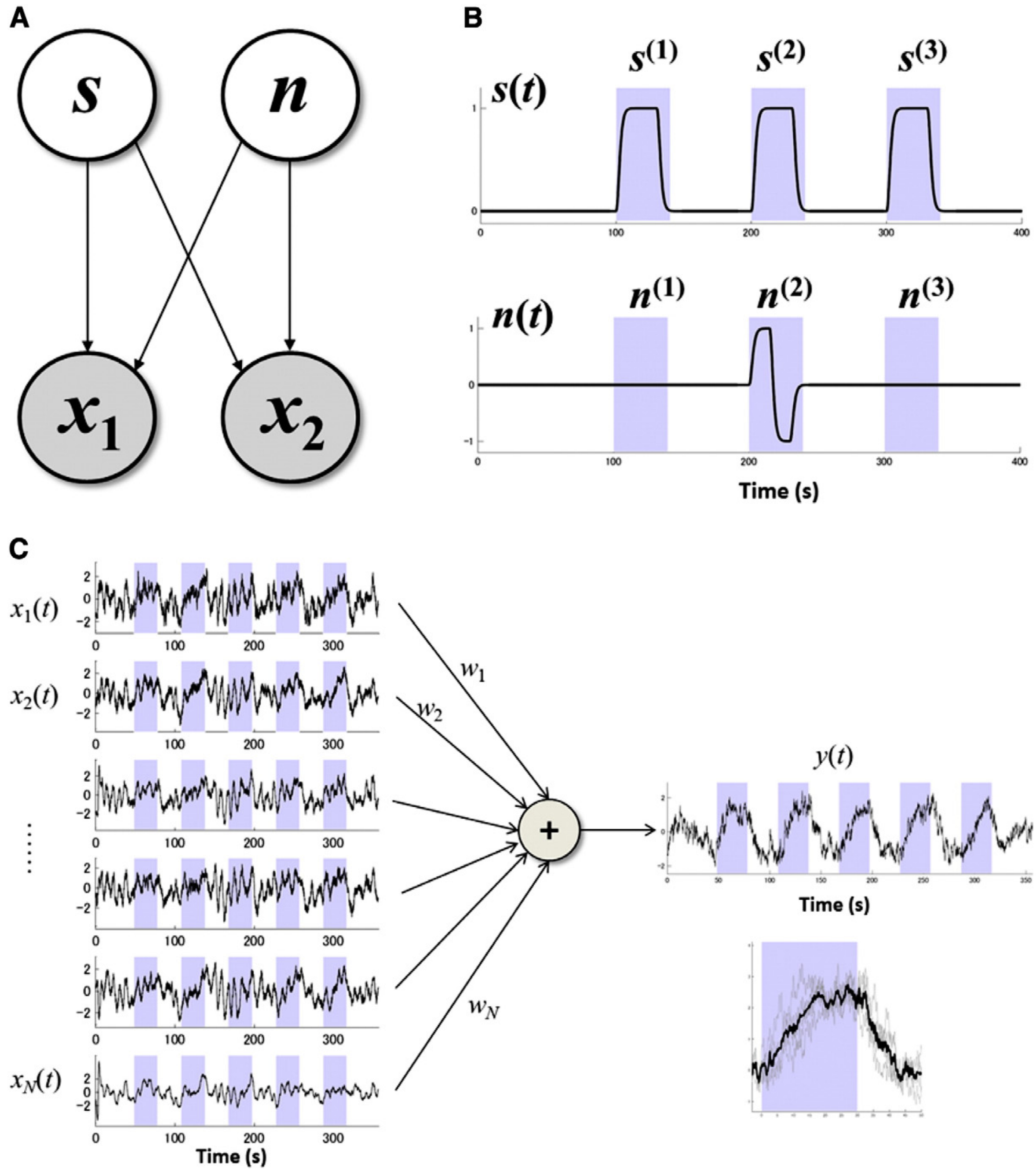

Fig. 1. (A) Time courses of task-related ($s(t)$) and task-unrelated ($n(t)$) components. Blue shaded areas indicate task blocks, and $s^{(i)}$ and $n^{(i)}$ are i-th block segments of $s(t)$ and $n(t)$, respectively. (B) A generative model of observation ($x_1(t)$ and $x_2(t)$) from task-related ($s(t)$) and task-unrelated ($n(t)$) components. (C) Schematics of TRCA. Multiple time series (left row) are summed with weights to give a single time course $y(t)$ (right). Shaded area in the time series indicate task blocks of a single task. The weights, or coefficients, are determined so as to maximize the sum of correlations or covariances of $y(t)$ between task blocks.

as illustrated in Fig. 1C. We will formulate this problem in two distinct but related ways; correlation maximization and covariance maximization.

Correlation maximization (CorrMax)

One such a measure of reproducibility is a correlation coefficient between k- and l-th blocks defined by

$$C_{kl} = \mathrm{Corr}\left(y^{(k)}(t), y^{(l)}(t)\right) = \frac{\sum_{i,j} w_i w_j \mathrm{Cov}\left(x_i^{(k)}(t), x_j^{(l)}(t)\right)}{\sqrt{\sum_{i,j} w_i w_j \mathrm{Cov}\left(x_i^{(k)}(t), x_j^{(k)}(t)\right)}\sqrt{\sum_{i,j} w_i w_j \mathrm{Cov}\left(x_i^{(l)}(t), x_j^{(l)}(t)\right)}}. \tag{6}$$

Here $y^{(k)}(t)$ and $x_i^{(k)}(t)$ denote a k-th block segment of $y(t)$ and$x_i(t)$, respectively. We propose to maximize the sum of correlation coefficients between all possible combinations of task blocks defined as

$$\begin{aligned}\sum_{\substack{k,l=1\\k\neq l}}^{K} C_{kl} &= \sum_{\substack{k,l=1\\k\neq l}}^{K} \mathrm{Corr}\left(y^{(k)}(t), y^{(l)}(t)\right)\\ &= \sum_{\substack{k,l=1\\k\neq l}}^{K} \frac{\sum_{i,j} w_i w_j \mathrm{Corr}\left(x_i^{(k)}(t), x_j^{(l)}(t)\right)}{\sqrt{\sum_{i,j} w_i w_j \mathrm{Corr}\left(x_i^{(k)}(t), x_j^{(k)}(t)\right)}\sqrt{\sum_{i,j} w_i w_j \mathrm{Corr}\left(x_i^{(l)}(t), x_j^{(l)}(t)\right)}}.\end{aligned} \tag{7}$$

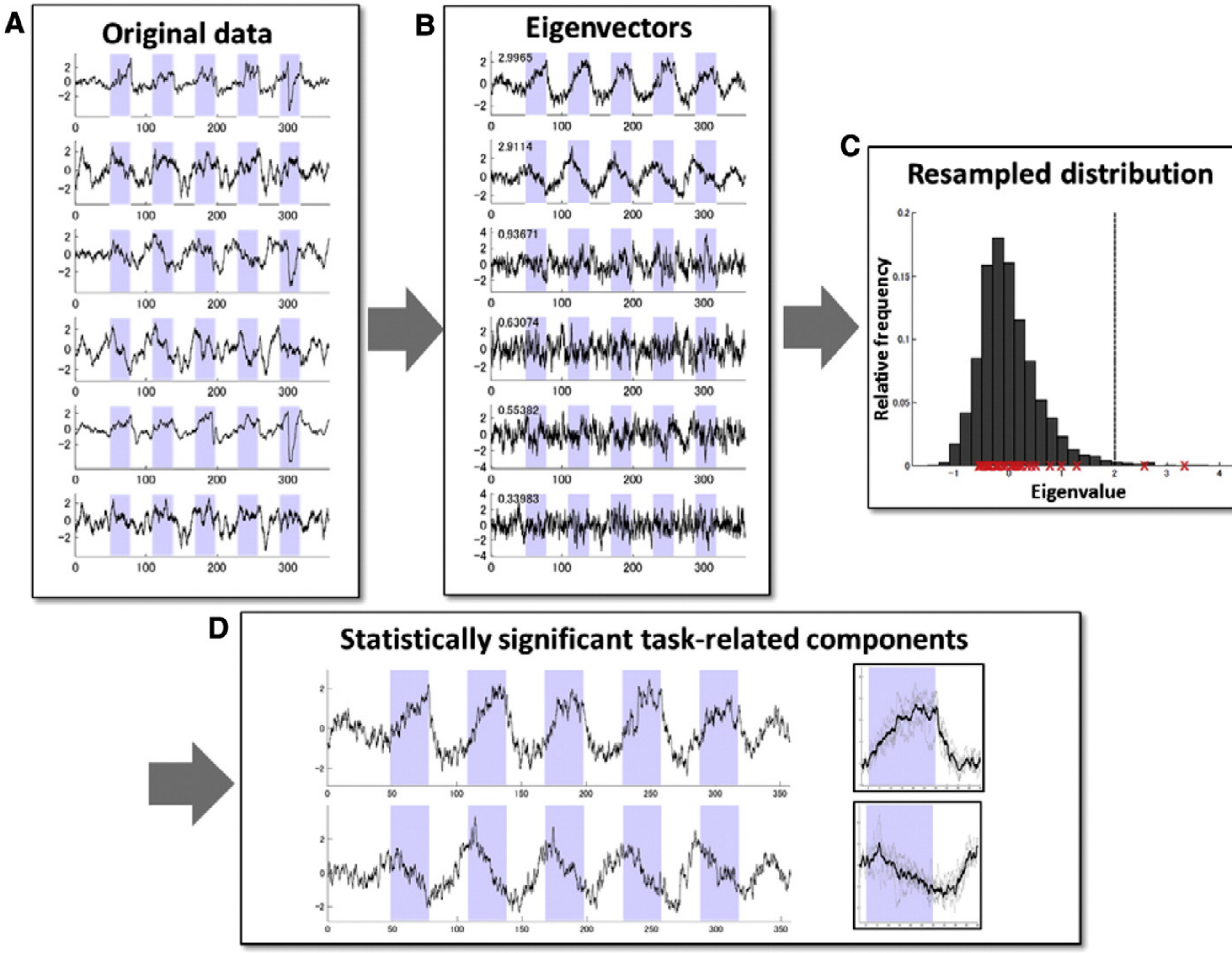

Fig. 2. Flow chart of TRCA. (A) Original multi-channel time series are decomposed into (B) task-related components using the algorithm presented in the 'Task-related component analysis: a basic formulation' section. (C) Statistical significance of the eigenvalues (red crosses on the horizontal axis) is evaluated using the resampling procedure in the 'Statistical test of task consistency' section. The dotted vertical line indicates a 99% confidence level. (D) Two eigenvalues outside the confidence level are selected as being significantly task-related in this case. The framed boxes on the right depict block averages of the two components, respectively. These figures were created with NIRS finger tapping data.

This objective function is invariant to a global rescaling of weight coefficients $w_i \to \alpha w_i$, so in order to bound the coefficients, the variance of $y(t)$ is normalized to one as

$$Var(y(t)) = \sum_{i,j=1}^{N} w_i w_j \mathrm{Cov}\left(x_i(t), x_j(t)\right) = \mathbf{w}^{\mathbf{T}}\mathbf{Q}\mathbf{w} = 1, \tag{8}$$

where $(\mathbf{Q})_{ij} \equiv \mathrm{Cov}(x_i(t), x_j(t))$. This formulation is referred to as correlation maximization (CorrMax). The objective function (Eq. (7)) is nonlinear in terms of the weight coefficients due to the quadratic terms in the denominators, so an analytical, closed-form solution cannot be expected. Instead, a numerical optimization algorithm (fmincon of MATLAB Optimization Toolbox, MathWorks, MA, U.S.A.) was used.

Covariance maximization (CovMax)

Although it is reasonable to maximize the sum of inter-block correlations (Eq. (7)), the computation for optimization does not have an analytically closed form, and more seriously, only a single task-related component is obtained. Instead of correlation coefficients, we propose an alternative way to maximize covariance between k-th and l-th blocks of $y(t)$:

$$\hat{C}_{kl} = \mathrm{Cov}\left(y^{(k)}(t), y^{(l)}(t)\right) = \sum_{i,j=1}^{N} w_i w_j \mathrm{Cov}\left(x_i^{(k)}(t), x_k^{(l)}(t)\right). \tag{9}$$

As in Eq. (7), all possible combinations of task blocks are summed as

$$\begin{aligned}\sum_{\substack{k,l=1\\k\neq l}}^{K} \hat{C}_{kl} &= \sum_{\substack{k,l=1\\k\neq l}}^{K} \mathrm{Cov}\left(y^{(k)}(t), y^{(l)}(t)\right)\\ &= \sum_{\substack{k,l=1\\k\neq l}}^{K} \sum_{i,j=1}^{N} w_i w_j \mathrm{Cov}\left(x_i^{(k)}(t), x_j^{(l)}(t)\right) = \mathbf{w}^{\mathbf{T}}\mathbf{S}\mathbf{w}.\end{aligned} \tag{10}$$

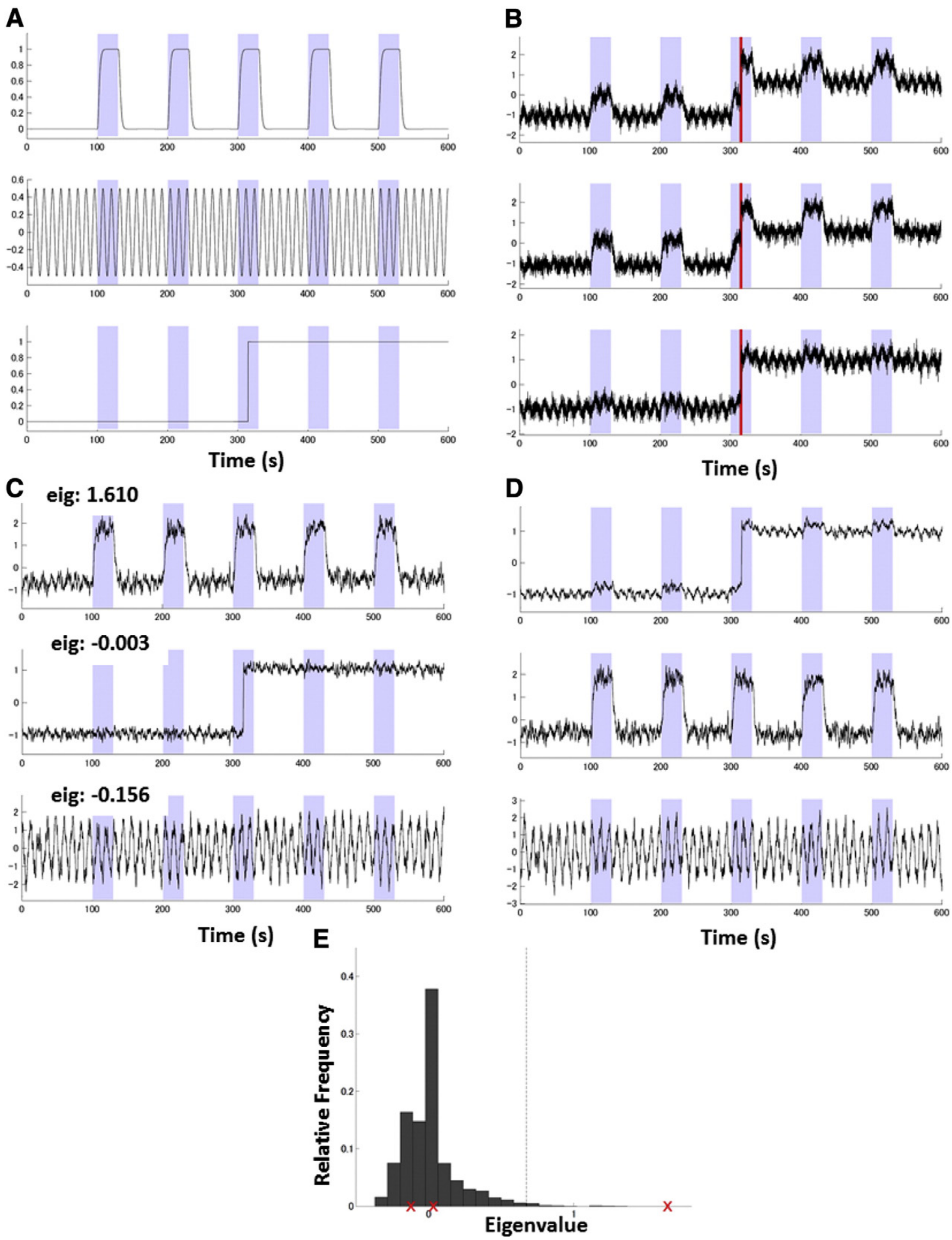

Fig. 3. Removal of a large movement artifact. (A) Input synthetic time series (from top to bottom: hemodynamic response, slow wave, and large-amplitude jerky movement). (B) Randomly mixed time courses. The red lines at 315 s during the third block indicate the moment of the sudden, large discontinuity. (C) Task related components with corresponding eigenvalues in a descending order and (D) independent components computed with the JADE algorithm. The components in panels C and D were moving averaged with a temporal window of 1 s after applying TRCA and JADE algorithms, respectively. (E) Eigenvalue distribution computed with randomized task onsets (gray bars) and original eigenvalues (red crosses). The vertical dashed line indicates 99% confidence interval.

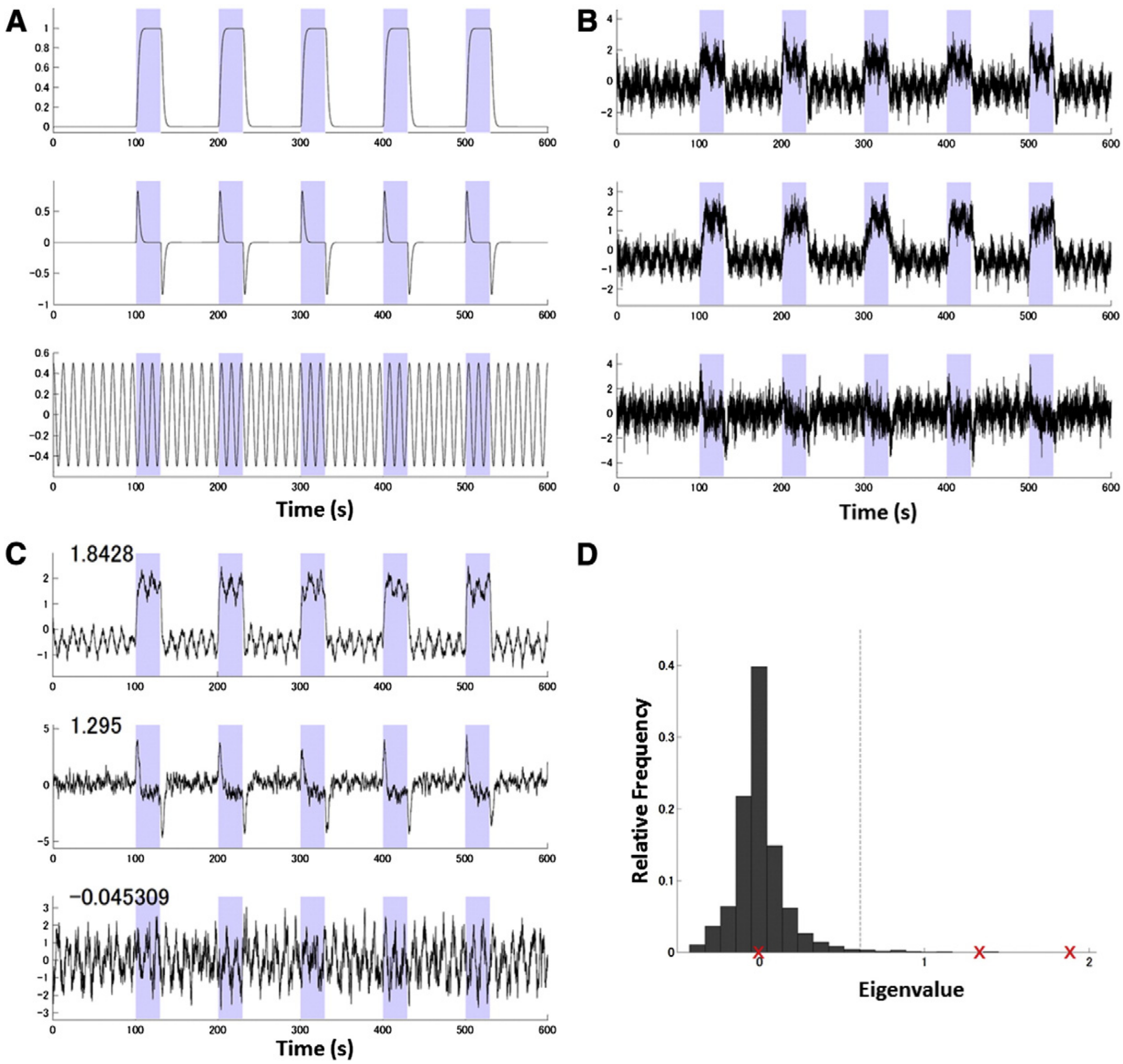

Fig. 4. Extraction of multiple task related components. (A) Input synthetic time series (from top to bottom: two task-related and one task-unrelated components). (B) Randomly mixed time courses. (C) Task-related components with corresponding eigenvalues. (D) Eigenvalue distribution computed with randomized task onsets (blue bars) and original eigenvalues (red crosses). The vertical dashed line indicates 99% confidence interval.

Here the symmetric matrix **S** is defined by

$$(S)_{ij} \equiv \sum_{\substack{k,l=1 \\ k \neq l}}^{K} \mathrm{Cov}\left(x_i^{(k)}(t), x_j^{(l)}(t)\right). \tag{11}$$

We propose to maximize the quantity defined in Eq. (10), which will be referred to as *task consistency*. This formulation is referred to as covariance maximization (CovMax). Note that inputs required by TRCA are only task block timings. As in the CorrMax algorithm, the normalization constraint (Eq. (8)) is imposed. Now the constrained optimization problem becomes a Rayleigh–Ritz eigenvalue problem:

$$\hat{\mathbf{w}} = \arg\max_{\mathbf{w}} \frac{\mathbf{w}^T \mathbf{S} \mathbf{w}}{\mathbf{w}^T \mathbf{Q} \mathbf{w}}. \tag{12}$$

With the help of the Rayleigh–Ritz theorem, the optimal coefficient vector is obtained as an eigenvector of the matrix $\mathbf{Q}^{-1}\mathbf{S}$. A Matlab function to solve this eigenvalue problem was included in Appendix A. Generally N eigenvectors of the matrix $\mathbf{Q}^{-1}\mathbf{S}$ are obtained, and correspondingly N components are obtained. Without loss of generality, task-related components are arranged in a descending order of associated eigenvalues. These eigenvalues can be used to statistically test whether the corresponding components are task-related or not, as discussed in the next subsection. Throughout this paper, the CovMax algorithm will be used unless otherwise stated.

Statistical test of task consistency

In order to assess how significantly task-related the components are, a statistical test must be introduced. One such measure is an eigenvalue λ of the matrix $\mathbf{Q}^{-1}\mathbf{S}$, which represents the value of cost function for the corresponding eigenvector $\hat{\mathbf{w}}$:

$$\hat{\mathbf{w}}^T \mathbf{S} \hat{\mathbf{w}} = \frac{\hat{\mathbf{w}}^T \mathbf{S} \hat{\mathbf{w}}}{\hat{\mathbf{w}}^T \mathbf{Q} \hat{\mathbf{w}}} = \frac{\lambda \hat{\mathbf{w}}^T \mathbf{Q} \hat{\mathbf{w}}}{\hat{\mathbf{w}}^T \mathbf{Q} \hat{\mathbf{w}}} = \lambda \quad \left(\because \mathbf{S}\hat{\mathbf{w}} = \lambda \mathbf{Q} \hat{\mathbf{w}}\right). \tag{13}$$

Therefore, the eigenvalue represents the task consistency among task blocks. If the original signals contain no task related components but just random variations, corresponding eigenvalues will be limited to a chance range.

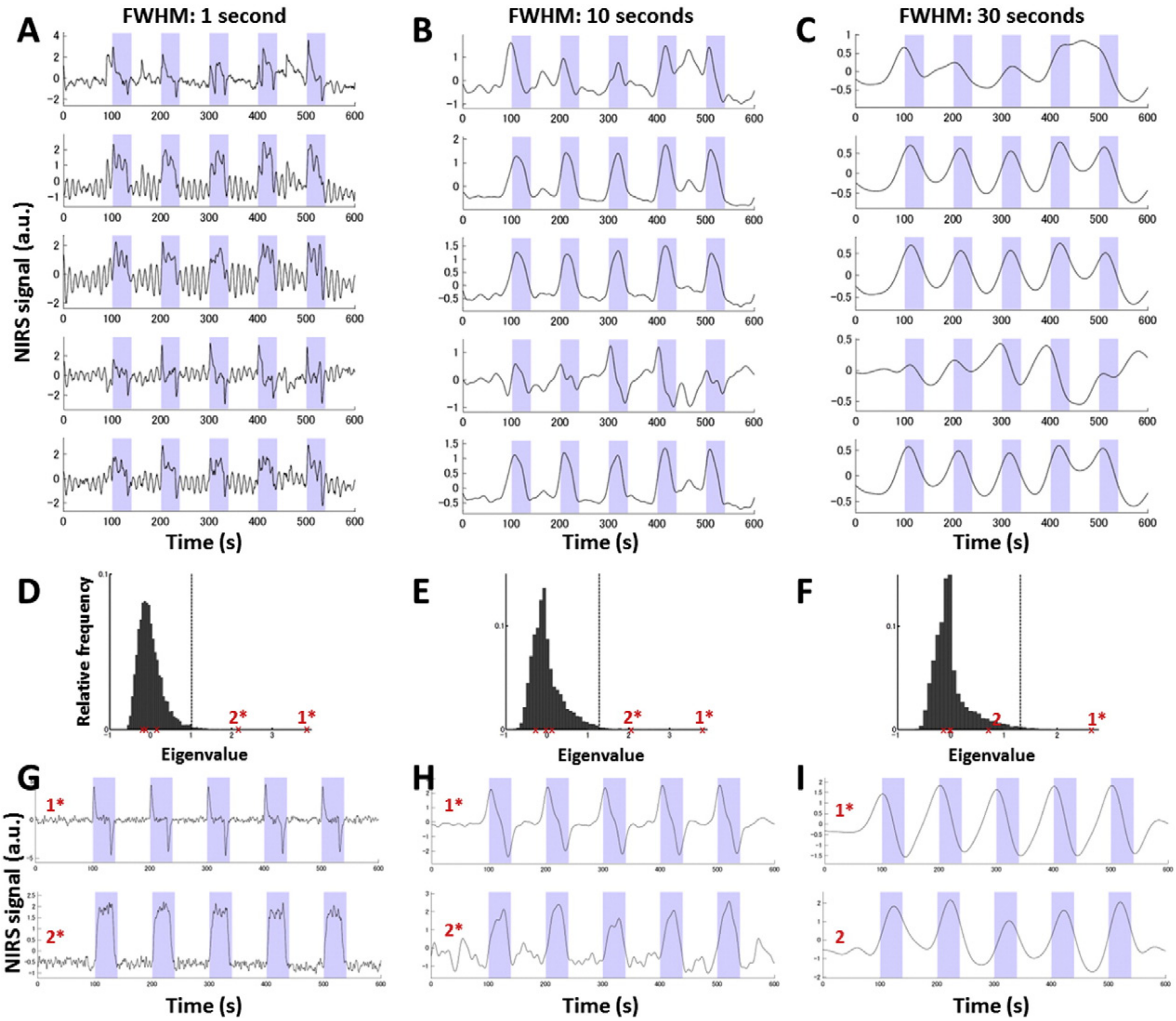

Fig. 5. Effect of temporal smoothing. (A, B, C) Input time courses smoothed with a Gaussian window of 1, 10 and 30 s FWHMs, respectively. (D, E, F) Eigenvalue distributions using randomized task onsets from the data in panels A, B and C, respectively. The red crosses on the horizontal axis represent the eigenvalues computed with the actual task onsets. The numbers indicate the corresponding components shown below in panels G, H or I. The asterisks denote statistical significance ($p<0.01$). (G, H, I) Extracted task-related components.

Mathematics of random matrices has been well investigated from the seminal work of Wigner, who explained the energy spectrum of an atomic nucleus as an eigenvalue distribution of a random matrix (Wigner, 1955, 1967). When x_i's are temporally uncorrelated random variables, the matrix $\mathbf{Q}$ in Eq. (8) is known as the Wishart matrix (Wishart, 1928) and its eigenvalue distribution is known in the limit of infinite N and T known as Marcenko–Pastur's quarter circle law (Marcenko and Pastur, 1967). This formula has been used to assess statistical significance of principal components of spike ensemble recording (Peyrache et al., 2010). The analytical formula assumes no temporal correlation between input time courses $\{x_i\}$, whereas there are considerable temporal autocorrelations in biological signals. Therefore, a statistical test based on the analytical formula is not appropriate for our case.

We here take a more practical and computational approach, in which the weight distribution when a null hypothesis is assumed is to use a non-parametric, permutation test. Our null hypothesis postulates that there is no task related component; therefore, instead of actual task onsets $\{t_k\}(k=1,\cdots,K)$, randomized task-block onsets (K time points sampled from a uniform distribution of entire experimental duration) can be used to compute the null distribution of weight coefficients. This gives the null distribution of weight coefficients, so a statistical significance of actual coefficients can be quantified by comparing with the null distribution. Eigenvalues outside a confidence interval of the null distribution can be regarded as being statistically significant, and corresponding eigenvectors can be regarded as being task related.

To summarize, TRCA consists of three computational steps: (1) computation of eigenvalues and eigenvectors of the matrix $\mathbf{Q}^{-1}\mathbf{S}$ with experimentally given periods of task blocks, (2) computation of the weight distribution with randomized periods of task blocks, and (3) selection of statistically significant task-related components. The procedure for computing task related components is schematically summarized in Fig. 2.

Effect of temporal smoothing and autocorrelation

Neuroimaging data such as BOLD signals in fMRI and oxy- and dexoy-hemoglobin concentration signals in NIRS contain considerable temporal autocorrelation due to inherent slow hemodynamic responses. Autocorrelation in the signals is enhanced by temporal smoothing, which is often employed for the purpose of artifact removal and the improvement of signal detection. In standard GLM methods, such autocorrelation leads to underestimation of the noise variance and hence to the inflation of estimated statistics (e.g., the t-statistic, which is inversely proportional to the noise variance). Considerable efforts have been made to develop methods to evaluate the degree of autocorrelation in data and to correct the statistic both in fMRI (Friston et al., 1994a, 1995, 2000; Worsley and Friston, 1995) and in NIRS (Fekete et al., 2011).

It is thus important to assess whether and how inflated autocorrelation due to inherent hemodynamics and temporal smoothing affects the results of the statistical analysis of TRCA because temporal smoothing induces spurious correlation and covariance. At first one might think that an appropriate correction is required when the method is applied to input time courses with considerable temporal autocorrelation because autocorrelation generally increases our covariance measure (Eq. (10)). However, as seen in Eq. (13), the optimal coefficient is determined as a tradeoff between the inter-block covariance (Eq. (10)) and the covariance of entire time courses (Eq. (8)), the latter of which also increases with temporal smoothing. The statistical test of TRCA uses the eigenvalues of the matrix $\mathbf{Q}^{-1}\mathbf{S}$ but not the individual matrices $\mathbf{Q}$ or $\mathbf{S}$. Whereas temporal smoothing increases the inter-block covariance (Eq. (10)) and the covariance of entire time course (Eq. (8)), the eigenvalues of the matrix $\mathbf{Q}^{-1}\mathbf{S}$ will not be affected. It is thus expected that the effect of temporal smoothing has a minimal impact on our analysis.

The above argument holds when the temporal scale of autocorrelation or temporal smoothing is small compared to the duration of task block or the entire experimental duration. There are two time scales in covariances of TRCA: the task duration for the matrix $\mathbf{S}$ and the entire experimental duration for the matrix $\mathbf{Q}$. If the scale of temporal smoothing increases beyond the duration of task block, the components of $\mathbf{S}$ matrix will be saturated whereas the components of $\mathbf{Q}$ matrix will still grow. Therefore, the eigenvalues of the matrix $\mathbf{Q}^{-1}\mathbf{S}$ will become smaller, and some of task-related components might not be able to survive. To summarize, the effect of temporal smoothing will be in effect if the smoothing scale becomes the same order of the task block. This consideration was verified with numerical simulations ('Effect of temporal smoothing' section).

Task-distinctive components

In practical applications such as brain–machine interface and brain decoding (Blankertz et al., 2008), it is often desirable to contrast neuroimaging data obtained in multiple task types. Once components related to each task are extracted, those will be used to infer corresponding cognitive states or to drive external devices such as a robot arm. Here we propose that a simple extension of TRCA can provide the most distinctive feature for binary task classification.

Let us consider two types of tasks, say A and B, which have K_{A} and K_{B} blocks with task periods $t\in[t_k^A, t_k^A+T]$ $(k=1,\cdots,K_A)$ and $t\in[t_k^B, t_k^B+T]$ $(k=1,\cdots,K_B)$, respectively. We construct a component that has maximal covariance between blocks of one task type and minimal covariance between blocks of different task types. As in the previous section, the covariance among task-A blocks

$$C_{kl}^{AA} = \mathrm{Cov}\left(y^{(k_A)}(t), y^{(l_A)}(t)\right) = \sum_{i,j} w_i w_j \mathrm{Cov}\left(x_i^{(k_A)}(t), x_j^{(l_A)}(t)\right) \tag{14}$$

and task-B blocks

$$C_{kl}^{BB} = \mathrm{Cov}\left(y^{(k_B)}(t), y^{(l_B)}(t)\right) = \sum_{i,j} w_i w_j \mathrm{Cov}\left(x_i^{(k_B)}(t), x_j^{(l_B)}(t)\right) \tag{15}$$

are to be maximized to give a task-related signal for both tasks A and B. We also require minimizing the covariance between task A and task B blocks,

$$\hat{C}_{kl}^{AB} = \mathrm{Cov}\left(y^{(k_A)}(t), y^{(l_B)}(t)\right) = \sum_{i,j} w_i w_j \mathrm{Cov}\left(x_i^{(k_A)}(t), x_j^{(l_B)}(t)\right) \tag{16}$$

and

$$\hat{C}_{kl}^{BA} = \mathrm{Cov}\left(y^{(k_B)}(t), y^{(l_A)}(t)\right) = \sum_{i,j} w_i w_j \mathrm{Cov}\left(x_i^{(k_B)}(t), x_j^{(l_A)}(t)\right). \tag{17}$$

Accordingly, the linear weighted sum that maximizes the intra-task covariances (Eqs. (14) and (15)) and minimizes the inter-task covariances (Eqs. (16) and (17)) will give the most distinctive time course between the two tasks. For this purpose, the objective function to be maximized now becomes

$$\sum_{\substack{k,l=1\\k\neq l}}^{K_A,K_B} \left(\hat{C}_{kl}^{AA} + \hat{C}_{kl}^{BB}\right) - \sum_{k,l=1}^{K_A,K_B} \left(\hat{C}_{kl}^{AB} + \hat{C}_{kl}^{BA}\right) = \mathbf{w}^T\mathbf{S}\mathbf{w}, \tag{18}$$

where the components of the matrix $\mathbf{S}$ is defined as

$$\begin{aligned}(\mathbf{S})_{ij} \equiv &\sum_{k\neq l}\left[\mathrm{Cov}\left(x_i^{(k_A)}(t), x_j^{(l_A)}(t)\right) + \mathrm{Cov}\left(x_i^{(k_B)}(t), x_j^{(l_B)}(t)\right)\right] \\ &-\sum_{k\neq l}\left[\mathrm{Cov}\left(x_i^{(k_A)}(t), x_j^{(l_B)}(t)\right) + \mathrm{Cov}\left(x_i^{(k_B)}(t), x_j^{(l_A)}(t)\right)\right].\end{aligned} \tag{19}$$

With this newly defined matrix $\mathbf{S}$, the coefficients are determined by solving the Rayleigh–Ritz problem (Eq. (12)), and corresponding components are referred to as task-distinctive components.

Data augmentation

The basic formulation of TRCA makes use of multi-channel signals obtained from a single modality, and task periods of a single task. In this sense, TRCA may be considered as a least supervised method. When additional, independent sources of information (such as body movement or respiration signals) are provided, it is desirable to make use of those sources in order to improve the task consistency. Here we show that a simple extension of TRCA can incorporate other sources of task-related and task-unrelated information step by step.

Suppose that, in addition to N-channel temporal signals denoted by $x_i(t)$ $(i=1,\cdots,N)$, additional, independent $\tilde{N}$ temporal signals denoted by $\tilde{x}_i(t)$ $(i=1,\cdots,\tilde{N})$ are given. These signals may, for example, represent task-unrelated artifacts such as body movement measured by an accelerometer or respiration measured by a respiratory belt, and we assume that $x_i(t)$'s are corrupted linearly by $\tilde{x}_i(t)$'s. Task consistency can be improved by appropriately subtracting task-unrelated components from $x_i(t)$. We propose that these two sets of temporal signals are augmented to form a new vector $\mathbf{X}$:

$$\mathbf{X}(t) = \left[x_1(t) \quad \cdots \quad x_N(t) \quad \middle| \quad \tilde{x}_1(t) \quad \cdots \quad \tilde{x}_{\tilde{N}}(t)\right]^T. \tag{20}$$

If we replace the original vector $\mathbf{x}$ in Eq. (5) with this augmented vector, task-related components can be computed as in the 'Task-related component analysis: a basic formulation' section. The additional signals provided by $\{\tilde{x}_i(t)\}$ can be regarded as supervised signals, so TRCA has a flexibility of incrementally integrating potentially informative signals.

Mapping of a task-related component

Once a statistically significant task-related component $y(t)$ is identified, the next task is to evaluate how each time course contains that task-related component. If input time courses are normalized to one, the correlation coefficient between i-th input time course and the task-related component is given as

$$\mathrm{E}[x_i(t)\cdot y(t)]. \tag{21}$$

By spatially aligning these dot products, a spatial map of the task-related component is obtained for individual subjects. Finally, spatial maps for multiple subjects are averaged channel by channel to obtain a subject-averaged spatial map (Singh et al., 2005).

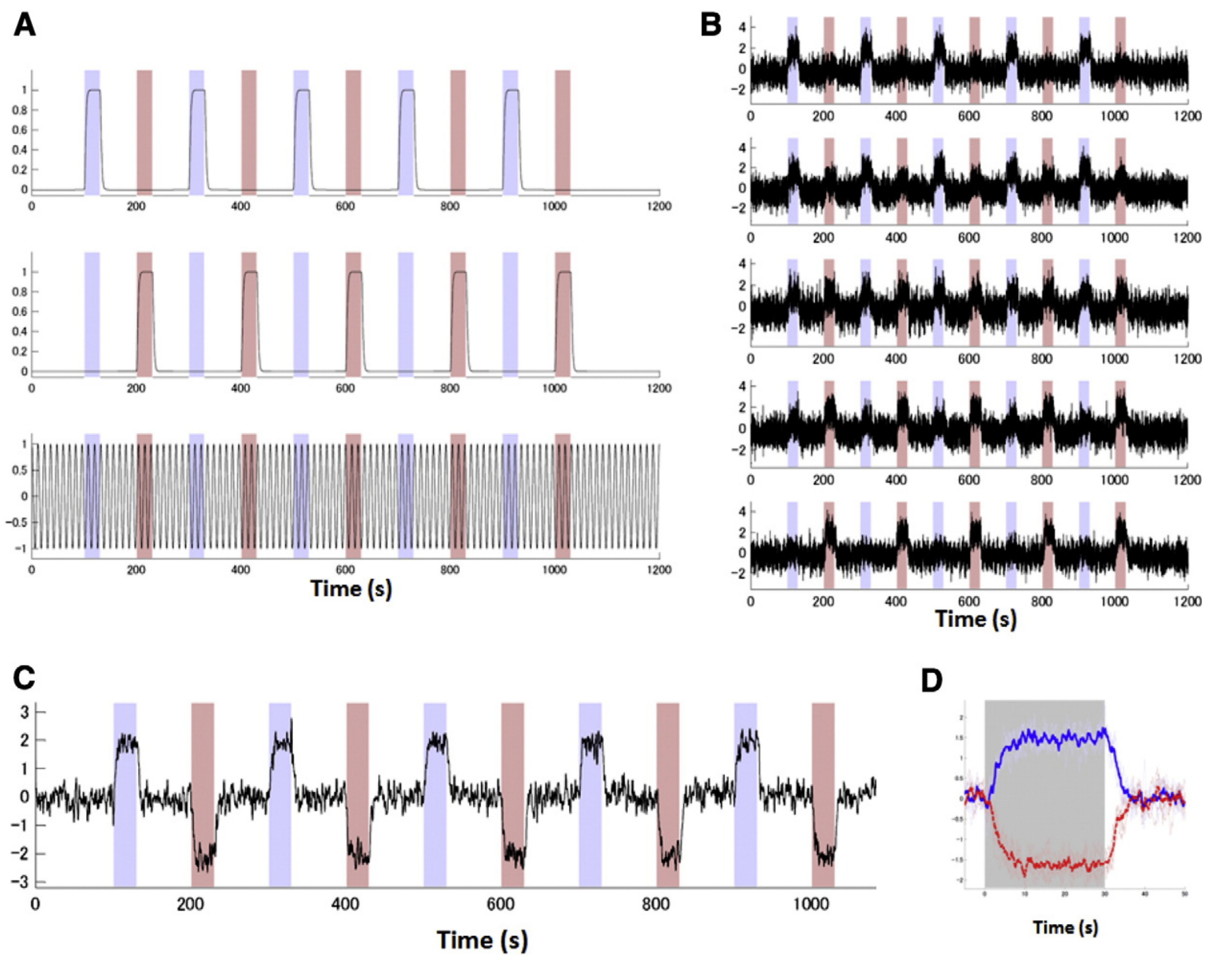

Fig. 6. Discriminative signal computed by TRCA. (A) Two task-related hemodynamics (top two) and task-unrelated slow wave (bottom). Blue- and red-shaded areas suggest task-A and task-B periods, respectively. (B) Five randomly mixed signals. (C) Most distinctive component and (D) its block averages.

Application to synthetic data

We have conducted four numerical simulations with synthetic data in order to illustrate how TRCA works: (1) a hemodynamic response corrupted with a physiological artifact and a motion artifact with large discontinuity ('Removal of motion artifact' section), (2) multiple task-related responses corrupted with physiological artifacts ('Extraction of multiple task-related components' section), (3) decorrelation of two-task signals ('Effect of temporal smoothing' section), and (4) incorporation of other source signals for artifact removal ('Task-distinctive component' section). These simulations were designed mainly for the following application to NIRS data. Details of synthetic data are summarized in Appendix B and Table 2. Whereas actual task periods were 30 s, extra 5 s prior to a block and 20 s after a block (therefore, totally 55 s) were included to compute correlation coefficients and covariances. This will ensure that task-related components have consistent signals not only during but also shortly before and after a task block.

NIRS finger tapping experiment

Although NIRS measures hemodynamic responses evoked by underlying neural responses like fMRI, the signal-to-noise ratio of NIRS is generally no better than that of fMRI (Cui et al., 2011). Also, NIRS data is corrupted with various systemic noises such as cardiac and respiratory signals, skin blood flow, and motion artifacts (Katura et al., 2006; Sato et al., 2006).

TRCA was then applied to NIRS data set of 29 subjects performing a finger tapping task, which was composed of five blocks, 30 s each. Details of experimental data were summarized in our previous publication (Katura et al., 2008; Sato et al., 2005). As in the synthetic case, 5 s before and 20 s after the task period were combined for the computation of correlation coefficients and covariances. Amplitudes of NIRS signals considerably vary channel-to-channel, so the standard deviation of each channel time course was normalized to one before applying TRCA. For the analysis of task-related components ('Task related components' section), the oxy-hemoglobin data for left- and right-finger tapping were analyzed independently. For the analysis of task-distinctive components ('Task-distinctive component' section), the data for left- and right-finger tapping were merged together as if they formed a single measurement, and both oxy- and deoxy-hemoglobin data were used.

Additional simulations and analyses

In order to assess the performance of our method, several additional simulations were performed with synthetic data with variable activation amplitudes, activation onsets, and sampling rates. Moreover, the method was tested with time courses of a simulated experiment of event-related design. Also, in order to evaluate how robust

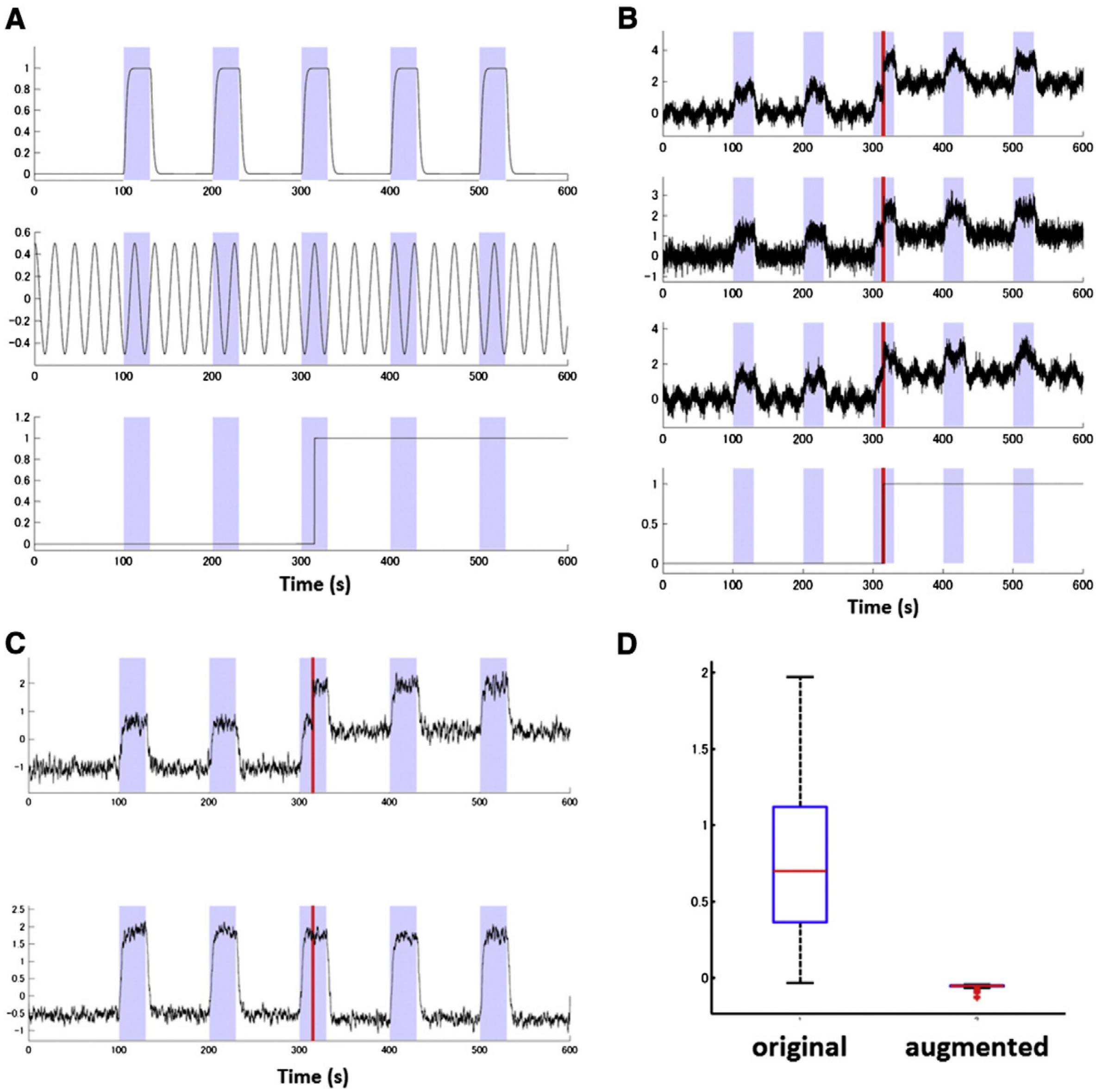

Fig. 7. Data augmentation in TRCA. (A) Three synthetic signals used for the simulation. (B) Randomly mixed signals (top three) and motion related signals (bottom). (C) Task-related component with the highest eigenvalue when the top three signals (top) or all the four signals (bottom) were used. (D) Box plot of the baseline-change indices of one-thousand repeated simulations.

task-related components were, TRCA was applied to NIRS data with reduced number of task blocks or channels. These results are summarized in the Supplementary data.

Results

Synthetic data

Four numerical experiments were conducted to assess our proposed method: removal of motion artifact ('Removal of motion artifact' section), extraction of multiple task-related components ('Extraction of multiple task-related components' section), effect of temporal smoothing ('Effect of temporal smoothing' section), distinctive components ('Task-distinctive component' section), and data augmentation ('Incorporation of augmented signals' section). Throughout the main text of this paper, TRCA was formulated and tested in a block-design experiment with non-overlapping task periods. An application to experiments of event-related design with overlapping task-related responses is argued in the Supplementary data.

Removal of motion artifact

Although NIRS is relatively tolerant to head and body movements compared to other neuroimaging modalities such as fMRI, its data still suffers from motion artifacts (Cui et al., 2010; Sato et al., 2006). In order to address how TRCA works for motion-contaminated data, synthetic data was created with a single task-related component and physical and physiological task-unrelated components (Fig. 3A). For the task-related component, five blocks of 30 s were included, and expected activations were computed by convolving with a standard hemodynamic response function (Boynton et al., 1996). The signals in Fig. 3A were randomly mixed to generate synthetic NIRS

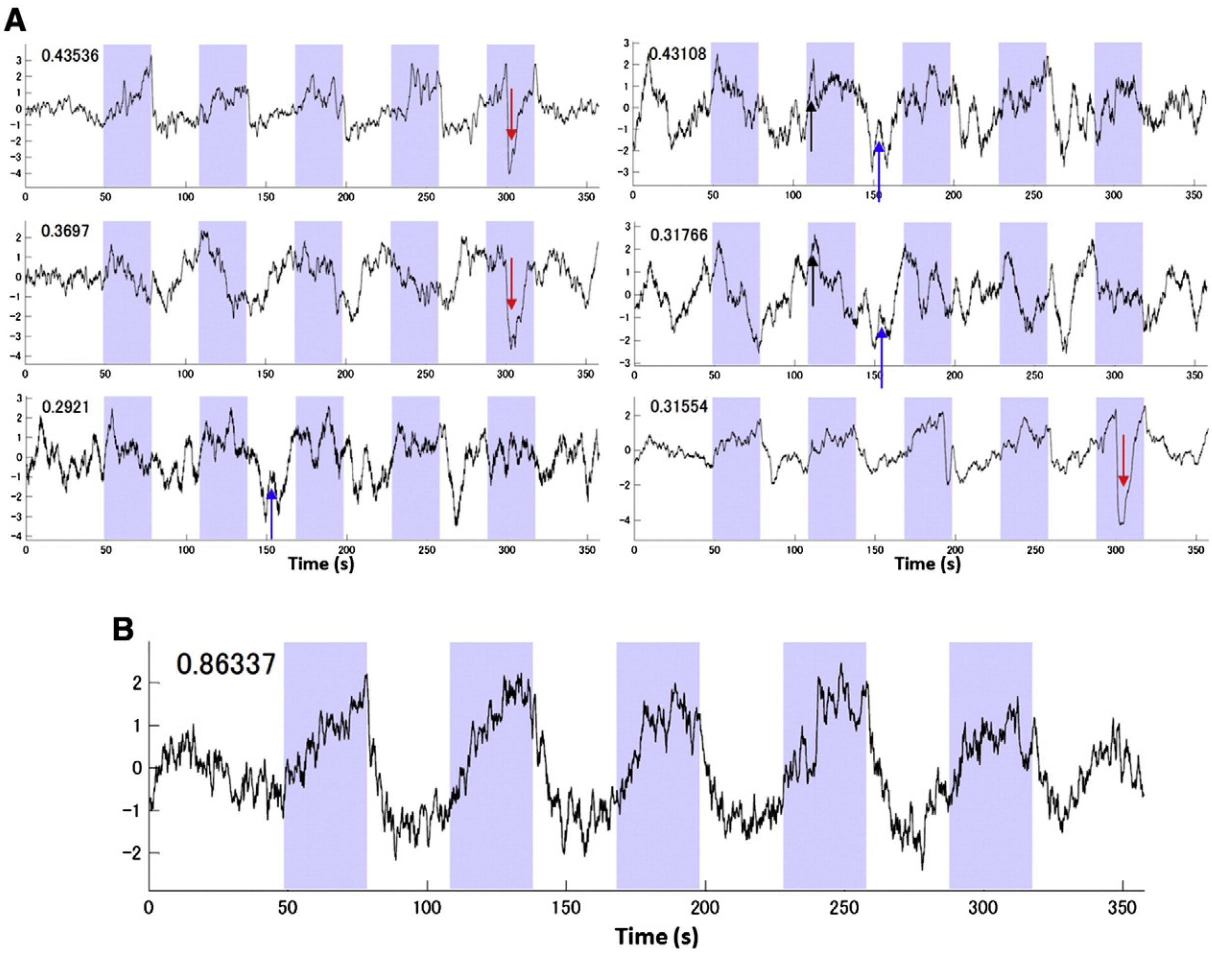

Fig. 8. Motion artifact removal by TRCA. (A) Time courses of NIRS channels with six largest inter-block correlation coefficients out of 24 channels. The numbers in upper left corners are corresponding correlation coefficients. Some artifacts that were possibly caused by body movements are indicated by blue arrows around 155 s and red arrows around 303 s. (B) Task-related component with the largest eigenvalue. The number at the upper left corner is a correlation coefficient among task blocks.

signals in Fig. 3B. An obvious jump at 315 s during the third block indicates that simple block averaging cannot remove such a large discontinuity.

We then applied TRCA to the synthetic data. The correlation matrices, **S** and **Q**, were computed by their definitions (Eqs. (11) and (8)). **Y** contains possible task-related components. We emphasize that the eigenvalues are the task consistency (Eq. (13)) of corresponding components. In other words, the reproducibility of a task-related component can be quantified by the corresponding eigenvalue.

Fig. 3C shows reconstructed task-related components in the order of decreasing eigenvalues. A statistical test indicated that only one component was statistically significant (Fig. 3E); the top row denotes the task-related component with the largest eigenvalue, and clearly this component recovered the hemodynamic response and did not suffer from the large discontinuity at 315 s. The other components were the jump and the physiological component, respectively, which are not regarded as task related due to their eigenvalues within the chance interval. Fig. 3D illustrates independent components computed by using the JADE algorithm (Cardoso, 1999). The jump component, hemodynamics component, and physiological component were separated, but an additional analysis step was needed to determine which component was task-related and task-unrelated.

Extraction of multiple task-related components

Generally the eigenvalue problem of Eq. (12) gives N possible solutions, and their task relatedness needs to be assessed by a statistical test on corresponding eigenvalues. By counting the number of statistically significant eigenvalues, therefore, the number of latent, task-related components can be estimated. Two task-related components and one task-unrelated component (Fig. 4A) were used to create synthetic data (Fig. 4B). Correspondingly, three potential task-related components were obtained (Fig. 4C). Their statistical significance was assessed by comparing with eigenvalues computed from block-shuffled inputs. There was one eigenvalue inside the confidence

Table 1
Numbers of statistically significant task-related components for left- and right-finger tapping experiment.

# Statistically significant components	# Subjects (left-finger tapping)	# Subjects (right-finger tapping)
0	1	1
1	8	6
2	19	22
3	1	0

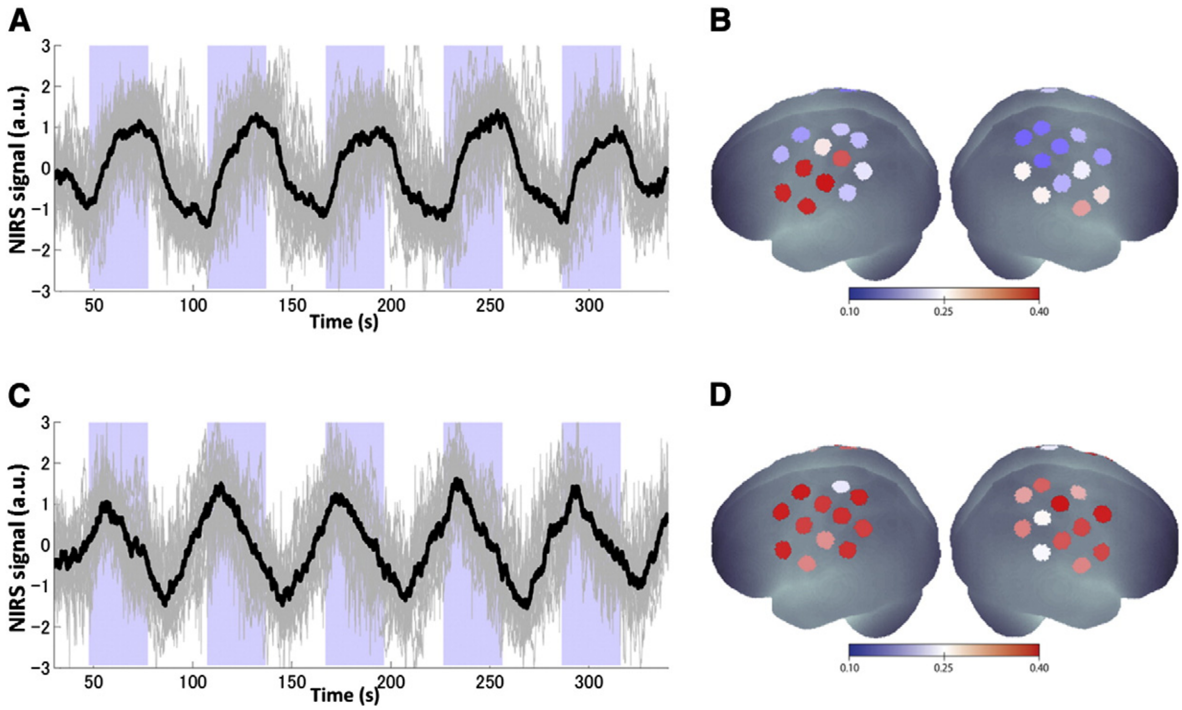

Fig. 9. (A) One TRC of right finger tapping and (B) the corresponding projection map. (C) Another TRC of right finger tapping and (D) the corresponding projection map.

interval, and there were two eigenvalues outside the confidence interval (Fig. 4D), thereby successfully recovering the original two task-related components and rejecting the remaining one as task-unrelated.

Effect of temporal smoothing

Whereas autocorrelation in time series reduces the noise variance and thus GLM analyses require an appropriate correction for the statistic, in the 'Effect of temporal smoothing and autocorrelation' section we provided an intuitive explanation of why autocorrelation will not matter in the case of TRCA, on condition that the time constant of autocorrelation is small compared with the duration of task block. To verify this intuition, a numerical simulation was performed by controlling the degree of autocorrelation with temporally smoothed synthetic data of various time scales. Five synthetic time courses were created from two task-related components

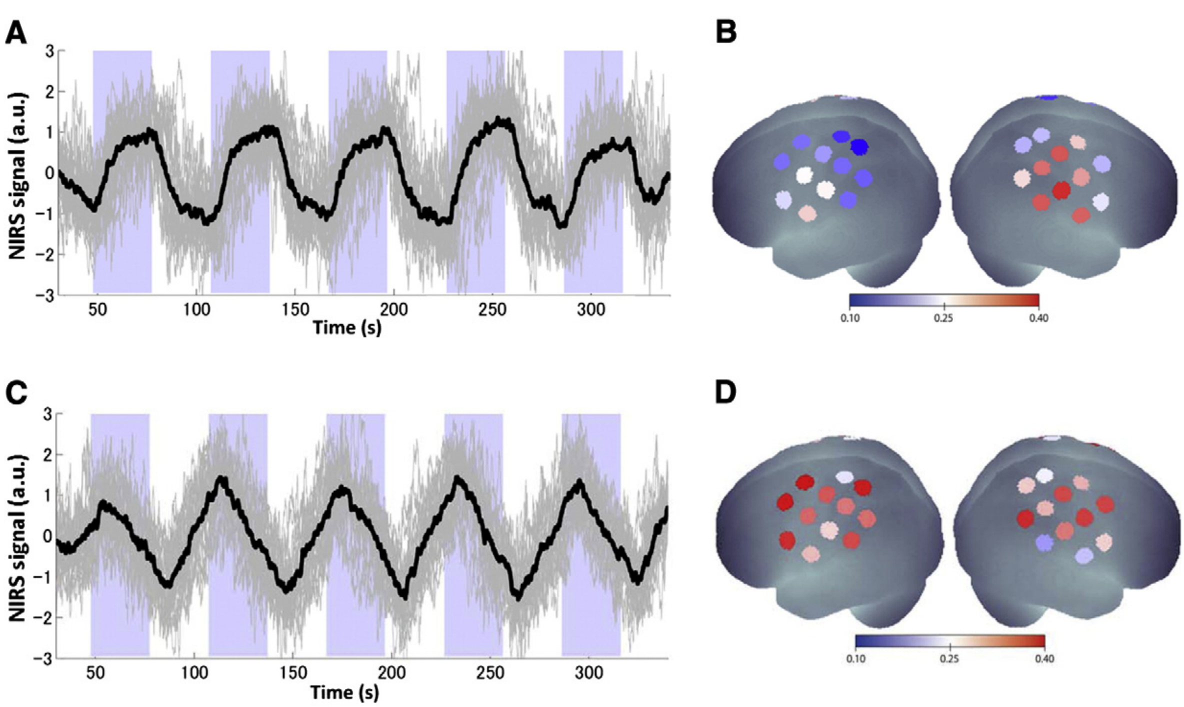

Fig. 10. (A) One TRC of left finger tapping and (B) the corresponding projection map. (C) Another TRC of left finger tapping and (D) the corresponding projection map.

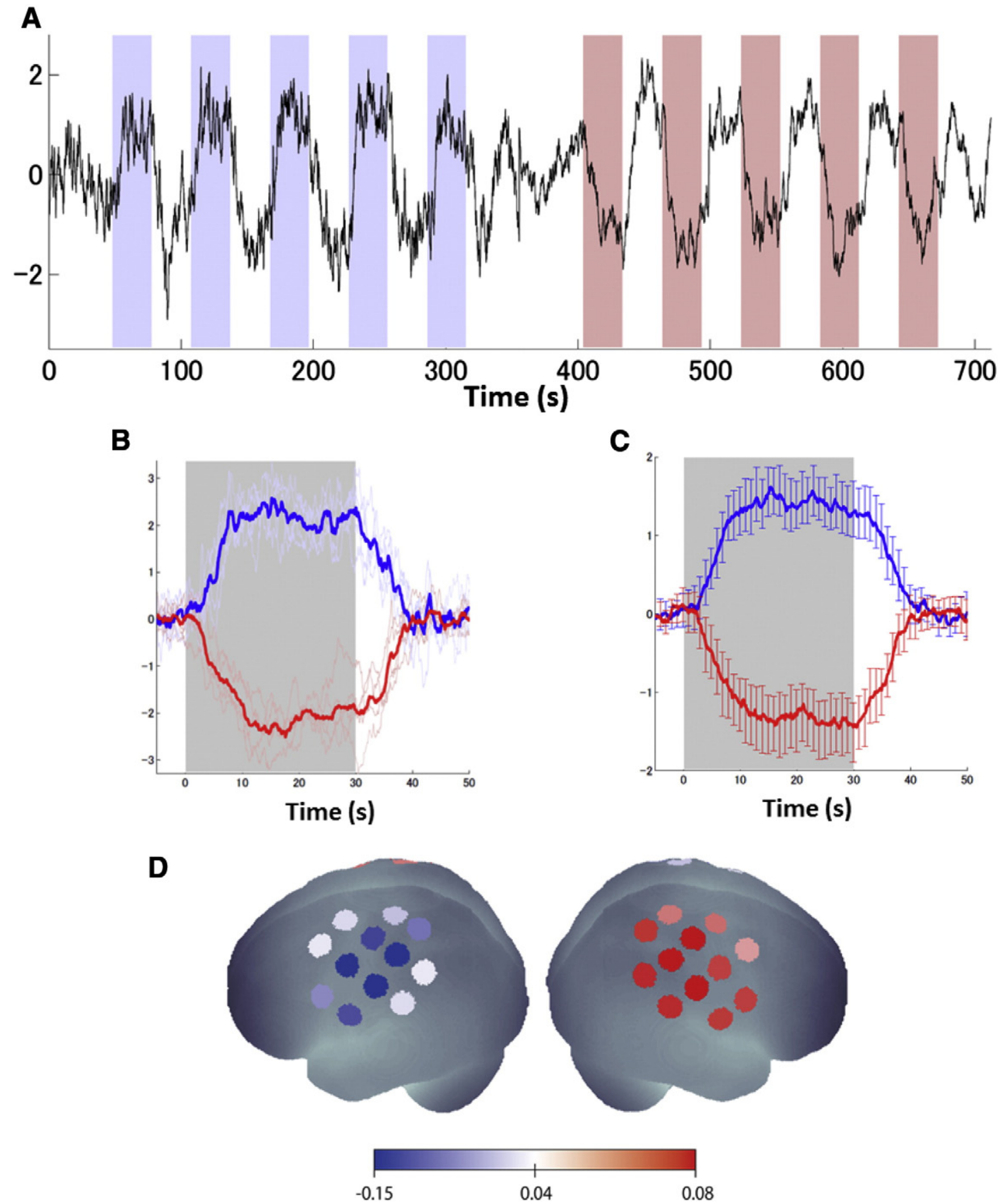

Fig. 11. (A) The most discriminatory time course computed from a representative subject. Blue and red shaded areas denote the task periods of right and left finger tapping, respectively. (B) Task-block average of the time course in panel A. Thin blue and red lines denote individual right and left finger tapping blocks, respectively, and thick blue and red lines are their averages. (C) Task block average computed from all subjects. Error bars indicate standard errors. (D) Corresponding project map averaged over all subjects.

corrupted with three task-unrelated components (see Section 1.3 of Supplementary data for details), followed by temporal smoothing with a Gaussian window of three values for full-width half-maximum or FWHM (1, 10, or 30 s) (Figs. 5A–C). In this simulation, the duration of a task block was 30 s, followed by 70 s of rest, thereby consisting of a periodic block design of 100 s. Details observed in the time courses in panel A became less apparent with the increase of the smoothing scale. For the three sets of data, the resampling distributions indicated that the two task-related components were correctly identified for the cases of 1 and 10 s FWHMs (Figs. 5D and E), whereas only one component was recovered for the case of 30 s FWHM (Fig. 5F), as expected from our intuitive explanation. Corresponding task-related components were shown in Figs. 5H–I. With the consideration in 'Effect of temporal smoothing and autocorrelation' section supported by this numerical result, we conclude that TRCA can safely be applied to data with considerable temporal autocorrelation if the scale of temporal autocorrelation is shorter than the duration of task block. This result also suggests that, if data contains autocorrelation due to hemodynamic response or temporal smoothing, the

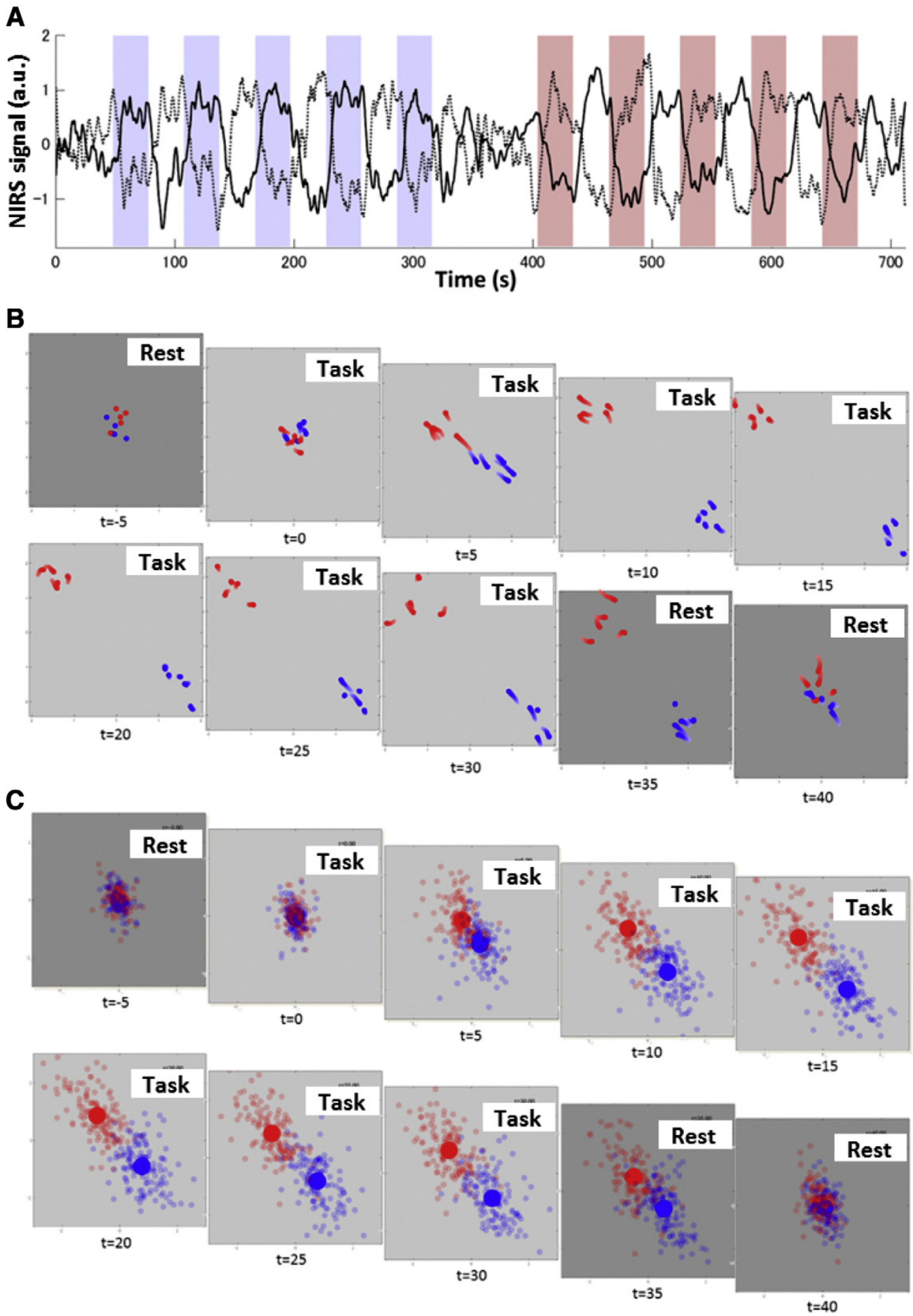

Fig. 12. (A) Most distinctive time courses computed using oxy- (solid line) and deoxy- (dotted line) hemoglobin NIRS signals of subject #12. Blue and red shaded areas denote the task periods of right and left finger tapping, respectively. (B) Snap shots of the distinctive components in panel A at t ranging from −5.0 to 40.0 in steps of 5 s. The horizontal and vertical axes denote distinctive components constructed from oxy- and deoxy-hemoglobin signals, respectively. Task period was indicated as light-gray background, and rest period as dark-gray background. (C) Snap shots of the distinctive components computed from all subjects at t ranging from −5.0 to 40.0 in steps of 5 s, using the same format of panel B. Translucent blue and red circles depict individual blocks, and large solid blue and red circles depict the center of mass.

task duration used for TRCA should be set sufficiently longer than the scale of autocorrelation, as discussed in designing an fMRI experiment (Friston et al., 2000).

Task-distinctive component

Often it is desirable to contrast activations from two distinct tasks, so synthetic data was created that contained two independent activations of two tasks (Fig. 6A). TRCA was applied to differentiate synthetic time courses that were composed of task-related components of two distinct tasks (Fig. 6B). A solution with the highest eigenvalue contained increases during blocks of one task and decreases during blocks of another task (Figs. 6C and D). Intra-task correlations were 0.93 (SD 0.0084) and 0.92 (SD 0.016) for task A and task B, respectively, and an inter-task correlation was −0.93 (SD 0.018).

Incorporation of augmented signals

In some cases in which signals and artifacts are mixed by a similar proportion to multiple time series, simple summation or subtraction between multiple time series cannot entirely cancel artifacts. Often additional sources of potential artifacts can be obtained by a separate and simultaneous recording such as cardiac, respiratory or motion measurements. TRCA is able to flexibly incorporate additional sources of artifact related components. Synthetic data was constructed from three signal time courses (Fig. 7A), and three random mixtures were used as inputs to TRCA (Fig. 7B, top three). Also, additional time course of a sudden jump was assumed (Fig. 7B, bottom). When only the three mixed time courses were used, often the discontinuity was not totally removed (Fig. 7C, top). This failure occurred when the individual time courses (top three in Fig. 7B) happened to contain hemodynamics and jump components in similar proportions. In contrast, TRCA applied to the augmented data could remove the jump component completely (Fig. 7C, bottom). The performance of the non-augmented and augmented methods was assessed by repeating this simulation with randomized mixture coefficients for one thousand times and by computing a baseline-change index defined by:

$$\frac{mean\left[y(t)\Big|_{t=315}^{t=600}\right]-mean\left[y(t)\Big|_{t=0}^{t=315}\right]}{std\left[y(t)\Big|_{t=0}^{t=600}\right]}. \tag{22}$$

The index takes zero if the jump component is completely removed. Fig. 7D shows a box plot of the indices, indicating that the performance of TRCA can be improved by incorporating additional sources of artifact information.

NIRS data of finger tapping

Task related components

An example of artifact removal is shown in Fig. 8. Time courses of six channels with largest correlation coefficients out of 24 channels (subject #23, left finger tapping) contain several artifacts that appeared to originate from body movements (Fig. 8A). These components occurred not reproducibly between task blocks, so TRCA optimized the weight coefficients so as to suppress these artifacts. The dominant TRC with the largest eigenvalue did not suffer these artifacts (Fig. 8B). Note also that there was an improvement in the correlation coefficient; the largest correlation coefficient among individual channels was 0.45 (top left in Fig. 8A), and the correlation coefficient of the dominant task-related component was 0.86. Also, this TRC appeared consistent with known properties of hemodynamic response in the motor cortex (Rao et al., 1996).

The same analysis was applied to all subjects. The numbers of statistically significant task-related components ranged from zero to three (Table 1). Most subjects had one or two components. There were a total of 99 task-related components (49 and 50 for right- and left-finger tapping) that were statistically significant. Since most subjects had at most two components, a k-means cluster analysis ($k=2$) with respect to Euclidean distance was performed in order to classify these dominant components.

Fig. 9 summarizes the two dominant TRCs for right-finger tapping. One TRC had a gradually changing time course similar to a conventional hemodynamics response; it gradually increased a few seconds after the task onsets and decreased a few seconds after the task offsets (Fig. 9A). Another TRC had a piece-wise linear time course; it peaked after a few seconds after the task onsets, linearly decreased until a few seconds after the task onsets, and then increased linearly (Fig. 9C). The inter-block correlations were 0.74 (SD 0.18) (Fig. 9A) and 0.56 (SD 0.17) (Fig. 9C), respectively. To visualize the contribution of the task-related components with the highest eigenvalues to original NIRS signals, projection coefficients (defined by a dot product $v_i = \mathrm{E}[y(t)\cdot x_i(t)]$, see 'Mapping of a task-related component' section) were first computed for individual subjects and then averaged over all subjects. One TRC projection map showed laterality to the contralateral hemisphere (Fig. 9B), whereas the other TRC map appeared to spread over the both hemispheres (Fig. 9D). We computed a laterality index (LI) defined by

$$\mathrm{LI} = \left. \left(\sum_{\substack{i\in\text{Left}\\ \text{Hemiphere}}} v_i - \sum_{\substack{i\in\text{Right}\\ \text{Hemiphere}}} v_i \right) \middle/ \sum_i |v_i| \right. \tag{23}$$

which takes a positive or negative value for left- or right-hemisphere dominant activation, respectively. Laterality indices were 0.17 (SD 0.30) and −0.0010 (SD 0.23) for Figs. 9B and D, respectively.

Similarly, Fig. 10 summarizes the two dominant TRCs for left-finger tapping. The inter-block correlations were 0.75 (SD 0.16) (Fig. 10A) and 0.63 (SD 0.16) (Fig. 10C), respectively. As in the case of the right-finger tapping, one component showed contralateral dominance (Fig. 10B) while another component appeared in both hemispheres (Fig. 10D). The laterality indices were −0.20 (SD 0.24) (Fig. 10B) and 0.060 (SD 0.28) (Fig. 10D), respectively. Furthermore, in order to see how robustly TRCA could detect these two dominant TRCs, TRCA was applied to a dataset with the reduced number of task blocks or NIRS channels. We found that TRCA could recover the two components robustly (see Supplementary Figs. 5 and 6).

The performance of the CovMax and CorrMax algorithms was evaluated by inter-block correlation coefficients. For comparison, correlations of all individual channels (29 (subjects) × 24 (channels) × 2 (conditions)) were computed. Medians of all individual channels, channels with maximal correlation per subject, and task related components derived by the CovMax and CorrMax algorithms were: 0.17, 0.50, 0.76 and 0.83 for left-finger tapping, and 0.18, 0.55, 0.71 and 0.85 for right-finger tapping. Computational time of the CovMax algorithm was 0.48 (SD 0.013) seconds per subject, and that of the CorrMax algorithm was 4.36 (SD 1.5592) seconds (Matlab, 2011b, MathWorks Inc. Intel Core2Duo CPU 3.0 GHz).

Table 2
Task-related and -unrelated components that were used for synthetic data.

Notation	Signal type	Functional form
$\boldsymbol{r_1(t)}$	Sustained hemodynamic response (task-related)	$s*h(t)$
$\boldsymbol{r_2(t)}$	Transient hemodynamic response (task-related)	$\frac{d}{dt}s*h(t)$
$\boldsymbol{r_3(t)}$	Mayer wave (task-unrelated)	$A_\mathrm{M}\sin\left(\frac{2\pi t}{T_\mathrm{M}}\right)$ $(A_\mathrm{M}=0.5, T_\mathrm{M}=12)$
$\boldsymbol{r_4(t)}$	Sudden discontinuity (task-unrelated)	$\Theta(t-315)=\begin{cases}1(t>315)\\0(t\leq315)\end{cases}$

Task-distinctive component

A task-distinctive component was extracted from right- and left-finger tapping data by using the algorithm presented in 'Effect of temporal smoothing and autocorrelation' section. Fig. 11A shows a representative time course from a single subject (subject #12), and Fig. 11B shows its block averages. Correlations between blocks of one task type (intra-task correlation) for this subject were 0.84 (SD 0.038) and 0.86 (SD 0.056) for left- and right-finger tapping, respectively, and correlation between blocks of different task types (inter-task correlation) was −0.85 (SD 0.044). In panel B, blocks of left-finger tapping showed elevated activations (blue lines) whereas blocks of right-finger tapping showed depressions (red lines). A group average of the same analysis was shown in Fig. 11C; intra-task correlations for all subjects were 0.53 (SD 0.25) and 0.50 (SD 0.27) for left- and right-finger tapping, respectively, and an inter-task correlation was −0.50 (SD 0.26). A projection map of this task-distinct component averaged over all subjects is illustrated in Fig. 11D.

The task-distinctive components provide a succinct description to classify two tasks from physiological measurements. NIRS has an advantage of simultaneous recording of oxy- and deoxy-hemoglobin, so TRCA was applied to both oxy- and deoxy-hemoglobin signals. Fig. 12A shows two task-distinctive components from the same subject in Fig. 11. The time courses of these task-distinctive components were projected onto a two-dimensional plane composed of oxy- and deoxy-hemoglobin signals (Fig. 12B). One sees that left- and right-finger tapping signals were inseparable before and after task period and separable during task period, indicating that these task-distinctive components provide a low-dimensional representation for classifying cognitive states. The same analysis was applied to all subjects (Fig. 12C).

Discussion

An analysis method based on inter-block reproducibility of biophysical signals was proposed. The reproducibility of signals among task blocks was measured with a sum of correlation coefficients (Eq. (7)) or covariances (Eq. (10)). In the latter case, the maximization of sum of covariances was reduced to a Rayleigh–Ritz eigenvalue problem, and a statistical significance of task relatedness was quantified by eigenvalues against a null hypothesis. Our task-related component analysis (TRCA) was applied to both synthetic and NIRS data. We demonstrated that TRCA is not sensitive to data with autocorrelation whose time scale is smaller than the duration of task block; this insensitivity to autocorrelation is advantageous when TRCA is generalized to other neuroimaging modalities or biophysical measurements.

Comparison with previous approaches

Several comments are made on this analysis method in comparison with previous approaches to neuroimaging data. First, this method differs from traditional, single-channel based analysis such as general linear models (Friston et al., 1994b), in which task related components are extracted within a single-channel time course. General linear models (GLMs) decompose individual voxel time courses into several presumed components, and the contribution of each component is assessed statistically. This approach implicitly assumes the fact that whole brain areas are entirely and uniformly sampled so GLMs should be able to detect task related voxels if there are any. These assumptions, however, may not hold for other functional neuroimaging modalities such as NIRS and EEG, whose sampling points are sparsely located only on the scalp. Our method, on the contrary, attempts to reconstruct a task related component from multiple-channel time courses with appropriate weight coefficients, and cortical areas responsible for the task consistency are mapped by evaluating a correlation between a task-related and original time courses. Also, the GLM approach depends critically on hypotheses of contributing time courses such as a shape of hemodynamic response (Plichta et al., 2007). On the other hand, our TRCA requires only onset timings of task blocks but not detailed time courses.

Second, the proposed method is, in mathematical formulation, similar to periodic component analysis, which is also formulated as a Rayleigh–Ritz eigenvalue problem (Monasterio et al., 2010; Sameni et al., 2008; Saul and Allen, 2001). We note, however, that our method is not restricted to periodic signals as long as task onsets are known, so it is flexibly applicable to an experimental design which uses non-periodic task cycles (see an application to an event-related experiment in Supplementary data).

Finally, our proposed analysis is an eigenvalues problem, so extracted components can be obtained with standard linear algebra methods that are computationally inexpensive. Moreover, statistical significance of an extracted component can be assessed by an associated eigenvalue, which implies the degree of inter-block covariances. This makes a contrast with independent component analysis, in which an additional procedure for quantifying how extracted independent components are task related is required. Our previous work applied ICA to the same dataset of finger tapping and found two task-related components that were similar to those reported in this work (Katura et al., 2008). But, in order to identify task-related components among candidate components separated by ICA, a threshold of inter-block correlation (0.2) was imposed, which was determined rather arbitrarily by hand. Another ICA study extracted an artifact component possibly related to skin blood flow by introducing an index describing spatial distribution of components (Kohno et al., 2007). They identified the most spatially uniform component as an artifact of skin blood flow, but what degree of uniformity is needed to be identified as such an artifact remains arbitrary. Our proposed method, in contrast, extracted two task-related components without introducing such arbitrary selection parameters.

Dominant task-related components

Our proposed method discovered statistically significant task-related components. One component (Figs. 8A and 9A) had a gradually changing time course and appeared in the hemisphere contralateral to tapping fingers (Figs. 8B and 9B). Therefore, we interpreted this component to be a hemodynamic response to finger tapping execution. Another component (Figs. 8C and 9C) had a piece-wise linear time course and its peaks occurred a few seconds after the task onsets. This component did not show a consistent hemispheric localization (Figs. 8D and 9D). In conventional NIRS analyses where multi-subject data was averaged on a channel-by-channel basis, this piece-wise linear component was not reported before to our knowledge. This component was not spatially reproducible but temporally reproducible, so the conventional analysis on channel-by-channel basis might not be able to detect this component. Our proposed TRCA based on temporal reproducibility could discover it.

One then will ask what this piece-wise component might represent. One interpretation is that it represents variable delays of hemodynamic responses in individual channels. Interestingly, we noticed that the temporal derivative of the hemodynamic response conspicuously resembled the piece-wise component (Supplementary Figs. 7A and B). In GLM analyses for fMRI data, it is a common practice to include a hemodynamic time course along with its temporal derivative so that delays in individual activations are adjusted. Although this may explain certain delays in activation onsets, we found that raw time courses of some channels closely resembled this piece-wise linear component (Supplementary Fig. 7C). Therefore, the delay interpretation itself cannot explain this piece-wise linear component.

Another interpretation of this component is hemodynamic fluctuations in the scalp that are estimated to be 10 to 20 times higher than those in cortical layers (Takahashi et al., 2011). There is considerable interest in the NIRS community in understanding hemoglobin changes that originate from neural and from systemic activities such as heart rate or blood pressure (Patel et al., 2011; Tachtsidis et al., 2009, 2010). Recently, Kirilina et al. (2012) reported oxy-hemoglobin time courses similar to our piece-wise linear component in a continuous performance task and a n-back working memory task. Functional NIRS combined with fMRI and peripheral physiological measurements revealed that these time courses were systemic artifacts whose origin was a task-evoked sympathetic arterial vasoconstriction followed by a decrease in venous volume in the scalp. In one study, Minati et al. (2011) quantified, with shallow- and deep-penetrating NIRS recording, the contribution of systemic blood pressure changes caused transiently by arm raising and concluded that systemic changes were reflected both in intra- and extracranial signals but with different patterns. In a related study, Saager et al. (2011) used two-detector NIRS with short and long separations and improved the signal-to-noise ratio by subtracting short-separation components from long-separation components. Takahashi et al. (2011) quantified the contribution of skin blood flow changes confounding in NIRS signal during a verbal fluency task by applying a pressure on the scalp between transmitting and detecting optodes. These studies employed certain specialized experiment settings such as two-distance optodes or pressure gauge, so it would be more convenient if confounding signals originating from systemic factors are identified and separated by a signal processing method.

To demonstrate this more explicitly, TRCA was applied to deoxy-hemoglobin as well as oxy-hemoglobin data. A recent study (Cui et al., 2010) suggested an artifact removal method based on the fact that the concentration changes of oxy- and deoxy-hemoglobin are negatively correlated for neural activation but not so for motion artifacts. We followed the same reasoning; if one component from oxy-hemoglobin is negatively correlated with another component from deoxy-hemoglobin, they are likely related to neural activation. Otherwise, positively or weakly correlated components are likely non-neural artifacts. We thus applied TRCA to deoxy-hemoglobin data (data not shown). One TRC in oxy-hemoglobin was negatively correlated with another TRC in deoxy-hemoglobin, therefore suggesting their neural origin. In contrast, one TRC in oxy-hemoglobin was positively correlated with another TRC in deoxy-hemoglobin, thereby indicating that they were not from neural activation. Thus TRCA can be a tool for separating components related to neural activation from those related to systemic factors.

We would like also to point out that a time course similar to ours was reported in a multi-wavelength intrinsic optical imaging experiment in which a behaving animal performed a visual attention task (Sirotin and Das, 2009; Sirotin et al., 2012) (there is, however, a controversy over whether or not the component Sirotin and Das reported was really task anticipatory and whether this component could be explained by electrophysiological signals, see Das and Sirotin, 2011; Handwerker and Bandettini, 2011a, 2011b; Kleinschmidt and Muller, 2010). Given the facts that the subjects were instructed that our task design was repetitive before the experiment (thus anticipatory) and that NIRS uses multiple wavelengths (thus containing information of not only oxygenation but also blood volume), it might not be surprising that NIRS signals contained some anticipatory signals similar to what Sirotin and Das had reported.

Possible extensions and future applications

This paper provided the basic formulation of task-related component analysis, and a few theoretical and practical extensions are considered here. First, whereas this paper proposed temporally reproducible signals as task-related components, spatially reproducible signals can also be considered as being task related. TRCA can be formulated so that an activation map has a maximal covariance between task blocks. Spatial TRCA may be applicable to fMRI data, in which temporal dimension (the number of temporal samplings) is usually much smaller than spatial dimensions (the number of voxels).

In our basic formulation of TRCA, the objective functions (Eqs. (7), (9) and (19)) contain the contributions of successive blocks and distant blocks equally, namely that the covariances between successive blocks and between distant blocks have the same weights in the objective functions. The assumption of our method is that components that are task-related should appear in the same manner in every task block, so in the basic formulation of our method the effect of changing hemodynamic responses in the course of an experiment has not been modeled. These equal contributions may be justified when no changes in activation during the course of an experiment are expected, as in simple tasks such as finger tapping. It is, however, desirable to extract adaptive changes of activation profiles during the course of the experiment, such as those related to learning or habituation. One way to model such effects could be to introduce an additional factor to account for the duration of the experiment:

$$\sum_{\substack{k,l=1 \\ k\neq l}}^{K} f_{kl}\mathrm{Cov}\left(y^{(k)}(t), y^{(l)}(t)\right) \tag{24}$$

If the factor (f_{kl}) is a decreasing function of the block distance $|k-l|$, the covariance between initial blocks and late blocks becomes less important. Therefore, the signals from initial and late blocks are not required to be very similar; only gradually signals that change block-by-block will be extracted.

Throughout this paper, we restrict ourselves to a linear model (Eq. (5)) to maximize the inter-block correlation or covariance. A higher reproducibility may be expected if input signals are mapped into a high dimensional feature space. A nonlinear extension may be possible by applying a kernel method, which has proved to be useful in areas such as kernel PCA (Mika et al., 1999b), kernel ICA (Bach and Jordan, 2003), kernel discriminant analysis (Mika et al., 1999a). Particularly, our linear formalism shares the same mathematics with Fisher linear discriminant analysis, so it is readily extendable to a nonlinear formalism with the help of kernel methods.

TRCA can also be applicable to multi-channel data that have several behaviorally relevant onsets. For example, a typical working-memory task contains stimulus-presentation timings and response timings of subjects. For example, a typical working-memory task contains stimulus-presentation timings and response timings of subjects. TRCA with stimulus-onsets and with response-onsets may reveal stimulus- and response-related activations, respectively. Our future study will address these limitations and extensions of TRCA.

Acknowledgments

We thank Drs. Naoki Tanaka and Masashi Kiguchi for encouraging discussions, Dr. Aniruddha Das for his help regarding the interpretation of NIRS signals, and three anonymous reviewers for their thoughtful comments. Thanks also go to Dr. Terrence J. Sejnowski for his comments on applications of independent component analysis to neuroimaging data. We acknowledge that Dr. Hiroshi Imamizu provided insightful comments on an earlier version of this manuscript.

Appendix A. MATLAB code

```
function [Y, V, D, S, C] = TRCA(X, t1, Nexp)

%% task-related component analysis
% Covariance Maximization (CovMax) algorithm
% X: data matrix (N channels * T time points)
% t1: task onsets (vector)
% Nexp: task duration (sampling unit)

Nchannel = size(X, 1);
Nblock = length(t1);

% computation of correlation matrices:
 S = zeros(Nchannel, Nchannel);
 for i=1:Nchannel
    for j=1:Nchannel
       for k=1:Nblock
          for l=1:Nblock
             if k~=l
                tk = t1(k); %onset of l-th block
                tl = t1(l);   %onset of l-th block
                xi = X(i, tk:tk+Nexp);
                xj = X(j, tl:tl+Nexp);
                S(i,j) = S(i,j) + (xi-mean(xi,2))*(xj-mean(xj,2))';
             end
          end
       end
    end
 end

X = X –repmat(mean(X,2),1,size(X,2));
Q = X*X';

% TRCA eigenvalue algorithm
[V, D] = eig(Q\S);
Y = V'*X;
```

Appendix B. Synthetic data

Here we describe some details of how synthetic data **X** was created for the four simulations in the 'Synthetic data' section. **X** represents an N (# channels) $\times T$ (# time points) matrix. N_s source signals were created and compiled into an $N_s \times T$ matrix **R**. These source signals could be task-related (i.e., hemodynamic responses) or -unrelated (i.e., systemic or movement-related artifacts). As in the 'Signal reconstruction from weighted linear summation' section, these source time series were randomly mixed up to give six synthetic time series (**X**: N (# channels) $*T$ (# time points)) as

$$\mathbf{X} = \mathbf{AR} + \boldsymbol{\xi}, \tag{B.1}$$

where **A** is the $N \times N_s$ mixing matrix. A Gaussian noise vector $\boldsymbol{\xi}$ of mean 0 and variance 0.3 was added. All time courses were sampled at 10 Hz. The four simulations ('Removal of motion artifact'–'Task-distinctive component' sections) differed in how the matrices **R** and **A** were created. Details of how the four synthetic data sets used in the main texts are summarized below and in Table 2.

B.1. Simulation in section 3.1.1

One hemodynamic response (r_1), one physiological component (r_3), and physical jump component (r_4) formed the matrix **R**.

$$\mathbf{R} = [r_1 \quad r_3 \quad r_4]^{\mathrm{T}}. \tag{B.2}$$

These time courses were 600 s long and sampled with 10 Hz (therefore, $T = 600$). For hemodynamic response (r_1), five task blocks of 30 s were placed at 100, 200, 300, 400 and 500 s, and a box-car function ($s(t)$) was defined to be one during the task periods and zero otherwise. A hemodynamic response function was adopted from Boynton et al. (1996):

$$h(t) = \left(\frac{t}{\tau}\right)^{n-1} \exp\left(-\frac{t}{\tau}\right) \Big/ (n-1)!\tau \tag{B.3}$$

where $\tau = 1.08$ and $n = 3$. Hemodynamic response (hence task related) was computed by convolving $s(t)$ and $h(t)$. For physiological component (r_3), an oscillatory signal of 0.0833 Hz (or 12 s period) was included to emulate the Mayer wave. For a physical artifact (r_4), a large jump at 315 s was included to emulate a motion artifact. The 3×3 mixing matrix **A** was created as

$$\mathbf{A} = \begin{pmatrix} 1 & 0 & 3 \\ 1 & 0 & 3 \\ 1 & 0 & 3 \end{pmatrix} + \begin{pmatrix} \eta_{11} & \eta_{12} & \eta_{13} \\ \eta_{21} & \eta_{22} & \eta_{23} \\ \eta_{31} & \eta_{32} & \eta_{33} \end{pmatrix} \tag{B.4}$$

where $\eta \sim N(0, 0.5^2)$.

B.2. Simulation in section 3.1.2

Five task blocks were included as in the simulation in the 'Removal of motion artifact' section. In addition to the sustained hemodynamic response function (r_1), another, transient task-related component (r_2) was introduced as a temporal derivative of Eq. (B.3). This phasic component was responsive positively to onset and negatively to offset of a task. The Mayer wave was also included, and the matrix **R** was defined as

$$\mathbf{R} = [r_1(t) \quad r_2(t) \quad r_3(t)]^{\mathrm{T}}. \tag{B.5}$$

The 3×3 matrix **A** was created as

$$\mathbf{A} = \begin{pmatrix} 0.5 & 0.5 & 0 \\ 0.5 & 0.5 & 0 \\ 0.5 & 0.5 & 0 \end{pmatrix} + \begin{pmatrix} \eta_{11} & \eta_{12} & \eta_{13} \\ \eta_{21} & \eta_{22} & \eta_{23} \\ \eta_{31} & \eta_{32} & \eta_{33} \end{pmatrix}, \tag{B.6}$$

where $\eta \sim N(0, 0.5^2)$.

B.3. Simulation in section 3.1.3

Ten task blocks, five for task A and the other five for task B, were created alternately from 100 to 1000 in steps of 100 s. The total duration was 1200 s sampled at 10 Hz. Two tasks were inserted alternatively; five task-A blocks of 30 s were placed starting at 100, 300, 500, 700 and 900 s, and five task-B blocks of 30 s starting at 200, 400, 600, 800 and1000 s. Accordingly, two box-car functions were constructed, and corresponding hemodynamic responses (r_1^A and r_1^B) were then created by convolving the box-car functions and Eq. (B.3). The Mayer-wave component was also added. The matrix **R** was

$$\mathbf{R} = \left[r_1^A(t) \quad r_1^B(t) \quad r_3(t) \right]^T, \tag{B.7}$$

and the 4×3 matrix **A** was

$$\mathbf{A} = \begin{pmatrix} 1.0 & 0.2 & \eta_{13} \\ 0.8 & 0.4 & \eta_{23} \\ 0.6 & 0.6 & \eta_{33} \\ 0.4 & 0.8 & \eta_{43} \\ 0.2 & 1.0 & \eta_{53} \end{pmatrix}, \tag{B.8}$$

where $\eta \sim N(0{,}0.3^2)$.

B.4. Simulation in section 3.1.4

A data matrix composed of three time courses in Fig. 7B (top three) was created in the same way as the 'Removal of motion artifact' section. In addition, an augmented data matrix composed of the three time courses plus one movement time course was created as:

$$\mathbf{X}(t) = [x_1(t) \quad x_2(t) \quad x_3(t) \quad r_4(t)]^T. \tag{B.9}$$

Appendix C. Supplementary data

Supplementary data to this article can be found online at http://dx.doi.org/10.1016/j.neuroimage.2012.08.044.

References

Amari, S., Cichocki, A., Yang, H.H., 1996. A new learning algorithm for blind signal separation. Advances in Neural Information Processing Systems, pp. 757–763.

Bach, F.R., Jordan, M.I., 2003. Kernel independent component analysis. J. Mach. Learn. Res. 3, 1–48.

Bell, A.J., Sejnowski, T.J., 1995. An information-maximization approach to blind separation and blind deconvolution. Neural Comput. 7, 1129–1159.

Blankertz, B., Tomioka, R., Lemm, S., Kawanabe, M., Muller, K.R., 2008. Optimizing spatial filters for robust EEG single-trial analysis. Signal Process. Mag. IEEE 25, 41–56.

Boynton, G.M., Engel, S.A., Glover, G.H., Heeger, D.J., 1996. Linear systems analysis of functional magnetic resonance imaging in human V1. J. Neurosci. 16, 4207.

Calhoun, V.D., Adali, T., Stevens, M.C., Kiehl, K.A., Pekar, J.J., 2005. Semi-blind ICA of fMRI: a method for utilizing hypothesis-derived time courses in a spatial ICA analysis. Neuroimage 25, 527–538.

Cardoso, J.F., 1999. High-order contrasts for independent component analysis. Neural Comput. 11, 157–192.

Cui, X., Bray, S., Reiss, A.L., 2010. Functional near infrared spectroscopy (NIRS) signal improvement based on negative correlation between oxygenated and deoxygenated hemoglobin dynamics. Neuroimage 49, 3039–3046.

Cui, X., Bray, S., Bryant, D.M., Glover, G.H., Reiss, A.L., 2011. A quantitative comparison of NIRS and fMRI across multiple cognitive tasks. Neuroimage 54, 2808–2821.

Das, A., Sirotin, Y.B., 2011. What could underlie the trial-related signal? A response to the commentaries by Drs. Kleinschmidt and Muller, and Drs. Handwerker and Bandettini. Neuroimage 55, 1413–1418 (discussion 1419–1422).

Fekete, T., Rubin, D., Carlson, J.M., Mujica-Parodi, L.R., 2011. The NIRS Analysis Package: noise reduction and statistical inference. PLoS One 6, e24322.

Friston, K.J., Jezzard, P., Turner, R., 1994a. Analysis of functional MRI time-series. Hum. Brain Mapp. 1, 153–171.

Friston, K.J., Holmes, A.P., Worsley, K.J., Poline, J.P., Frith, C.D., Frackowiak, R.S.J., 1994b. Statistical parametric maps in functional imaging: a general linear approach. Hum. Brain Mapp. 2, 189–210.

Friston, K.J., Holmes, A.P., Poline, J.B., Grasby, P.J., Williams, S.C., Frackowiak, R.S., Turner, R., 1995. Analysis of fMRI time-series revisited. Neuroimage 2, 45–53.

Friston, K.J., Josephs, O., Zarahn, E., Holmes, A.P., Rouquette, S., Poline, J., 2000. To smooth or not to smooth? Bias and efficiency in fMRI time-series analysis. Neuroimage 12, 196–208.

Handwerker, D.A., Bandettini, P.A., 2011a. Simple explanations before complex theories: alternative interpretations of Sirotin and Das' observations. Neuroimage 55 (4), 1419–1422.

Handwerker, D.A., Bandettini, P.A., 2011b. Hemodynamic signals not predicted? Not so: a comment on Sirotin and Das (2009). Neuroimage 55, 1409–1412.

Hyvarinen, A., Oja, E., 1997. A fast fixed-point algorithm for independent component analysis. Neural Comput. 9, 1483–1492.

Katura, T., Tanaka, N., Obata, A., Sato, H., Maki, A., 2006. Quantitative evaluation of interrelations between spontaneous low-frequency oscillations in cerebral hemodynamics and systemic cardiovascular dynamics. Neuroimage 31, 1592–1600.

Katura, T., Sato, H., Fuchino, Y., Yoshida, T., Atsumori, H., Kiguchi, M., Maki, A., Abe, M., Tanaka, N., 2008. Extracting task-related activation components from optical topography measurement using independent components analysis. J. Biomed. Opt. 13, 054008.

Kirilina, E., Jelzow, A., Heine, A., Niessing, M., Wabnitz, H., Bruhl, R., Ittermann, B., Jacobs, A.M., Tachtsidis, I., 2012. The physiological origin of task-evoked systemic artefacts in functional near infrared spectroscopy. Neuroimage 61, 70–81.

Kleinschmidt, A., Muller, N.G., 2010. The blind, the lame, and the poor signals of brain function—a comment on Sirotin and Das (2009). Neuroimage 50, 622–625.

Kohno, S., Miyai, I., Seiyama, A., Oda, I., Ishikawa, A., Tsuneishi, S., Amita, T., Shimizu, K., 2007. Removal of the skin blood flow artifact in functional near-infrared spectroscopic imaging data through independent component analysis. J. Biomed. Opt. 12, 062111.

Lin, Q.-H., Liu, J., Zheng, Y.-R., Liang, H., Calhoun, V.D., 2010. Semiblind spatial ICA of fMRI using spatial constraints. Hum. Brain Mapp. 31, 1076–1088.

Makeig, S., Bell, A.J., Jung, T.P., Sejnowski, T.J., 1996. Independent component analysis of electroencephalographic data. Advances in Neural Information Processing Systems, pp. 145–151.

Marcenko, V.A., Pastur, L.A., 1967. Distribution of eigenvalues for some sets of random matrices. Math. USSR-Sb. 1, 457.

McKeown, M.J., Sejnowski, T.J., 1998. Independent component analysis of fMRI data: examining the assumptions. Hum. Brain Mapp. 6, 368–372.

Mika, S., Scholkopf, B., Smola, A.J., Muller, K.R., Scholz, M., Ratsch, G., 1999a. Kernel PCA and de-noising in feature spaces: Advances in Neural Information Processing Systems, 11, pp. 536–542.

Mika, S., Ratsch, G., Weston, J., Scholkopf, B., Mullers, K.R., 1999b. Fisher discriminant analysis with kernels. Neural Networks for Signal Processing IX: Proceedings of the 1999 IEEE Signal Processing Society Workshop (Cat No98TH8468).

Minati, L., Kress, I.U., Visani, E., Medford, N., Critchley, H.D., 2011. Intra- and extra-cranial effects of transient blood pressure changes on brain near-infrared spectroscopy (NIRS) measurements. J. Neurosci. Methods 197, 283–288.

Monasterio, V., Clifford, G.D., Laguna, P., Martinez, J.P., 2010. A multilead scheme based on periodic component analysis for T-wave alternans analysis in the ECG. Ann. Biomed. Eng. 38, 2532–2541.

Nakada, T., Suzuki, K., Fujii, Y., Matsuzawa, H., Kwee, I.L., 2000. Independent component-cross correlation-sequential epoch (ICS) analysis of high field fMRI time series: direct visualization of dual representation of the primary motor cortex in human. Neurosci. Res. 37, 237–244.

Nakamura, H., Yoshida, M., Kotani, M., Akazawa, K., Moritani, T., 2004. The application of independent component analysis to the multi-channel surface electromyographic signals for separation of motor unit action potential trains: part I—measuring techniques. J. Electromyogr. Kinesiol. 14, 423–432.

Patel, S., Katura, T., Maki, A., Tachtsidis, I., 2011. Quantification of systemic interference in optical topography data during frontal lobe and motor cortex activation: an independent component analysis. Adv. Exp. Med. Biol. 701, 45–51.

Peyrache, A., Benchenane, K., Khamassi, M., Wiener, S.I., Battaglia, F.P., 2010. Principal component analysis of ensemble recordings reveals cell assemblies at high temporal resolution. J. Comput. Neurosci. 29, 309–325.

Plichta, M.M., Heinzel, S., Ehlis, A.C., Pauli, P., Fallgatter, A.J., 2007. Model-based analysis of rapid event-related functional near-infrared spectroscopy (NIRS) data: a parametric validation study. Neuroimage 35, 625–634.

Rao, S.M., Bandettini, P.A., Binder, J.R., Bobholz, J.A., Hammeke, T.A., Stein, E.A., Hyde, J.S., 1996. Relationship between finger movement rate and functional magnetic resonance signal change in human primary motor cortex. J. Cereb. Blood Flow Metab. 16, 1250–1254.

Saager, R.B., Telleri, N.L., Berger, A.J., 2011. Two-detector Corrected Near Infrared Spectroscopy (C-NIRS) detects hemodynamic activation responses more robustly than single-detector NIRS. Neuroimage 55, 1679–1685.

Sameni, R., Jutten, C., Shamsollahi, M.B., 2008. Multichannel electrocardiogram decomposition using periodic component analysis. IEEE Trans. Biomed. Eng. 55, 1935–1940.

Sato, H., Fuchino, Y., Kiguchi, M., Katura, T., Maki, A., Yoro, T., Koizumi, H., 2005. Intersubject variability of near-infrared spectroscopy signals during sensorimotor cortex activation. J. Biomed. Opt. 10, 44001.

Sato, H., Tanaka, N., Uchida, M., Hirabayashi, Y., Kanai, M., Ashida, T., Konishi, I., Maki, A., 2006. Wavelet analysis for detecting body-movement artifacts in optical topography signals. Neuroimage 33, 580–587.

Saul, L.K., Allen, J.B., 2001. Periodic component analysis: an eigenvalue method for representing periodic structure in speech. Advances in Neural Information Processing Systems, pp. 807–813.

Sirotin, Y.B., Das, A., 2009. Anticipatory haemodynamic signals in sensory cortex not predicted by local neuronal activity. Nature 457, 475–479.

Sirotin, Y.B., Cardoso, M., Lima, B., Das, A., 2012. Spatial homogeneity and task-synchrony of the trial-related hemodynamic signal. Neuroimage 59, 2783–2797.

Tachtsidis, I., Leung, T.S., Chopra, A., Koh, P.H., Reid, C.B., Elwell, C.E., 2009. False positives in functional nearinfrared topography. Oxygen Transp. Tissue XXX, 307–314.

Tachtsidis, I., Koh, P.H., Stubbs, C., Elwell, C.E., 2010. Functional optical topography analysis using statistical parametric mapping (SPM) methodology with and without physiological confounds. Oxygen Transp. Tissue XXXI, 237–243.

Takahashi, T., Takikawa, Y., Kawagoe, R., Shibuya, S., Iwano, T., Kitazawa, S., 2011. Influence of skin blood flow on near-infrared spectroscopy signals measured on the forehead during a verbal fluency task. Neuroimage 57, 991–1002.
Wigner, E.P., 1955. Characteristic vectors of bordered matrices with infinite dimensions. Ann. Math. 62, 548–564.
Wigner, E.P., 1967. Random matrices in physics. SIAM Rev. 9, 1–23.
Wishart, J., 1928. The generalised product moment distribution in samples from a normal multivariate population. Biometrika 20, 32–52.
Worsley, K.J., Friston, K.J., 1995. Analysis of fMRI time-series revisited—again. Neuroimage 2, 173–181.